SUMMARY OF CALCITE AND OPAL DEPOSITS IN THE EXPLORATORY STUDIES FACILITY AND ESTIMATES OF THE DISTRIBUTION AND ISOTOPIC COMPOSITIONS OF THESE MINERALS ALONG THE EAST-WEST CROSS DRIFT ALIGNMENT, YUCCA MOUNTAIN, NEVADA

DRAFT REPORT

U.S. GEOLOGICAL SURVEY

Open-File Report 98-xxx

Prepared in cooperation with the
NEVADA OPERATIONS OFFICE,
U.S. DEPARTMENT OF ENERGY, under
Interagency Agreement DE-AI08-97NV12033

9809240211 980922
PDR WASTE
WM-11 PDR
102

SUMMARY OF CALCITE AND OPAL DEPOSITS IN THE EXPLORATORY STUDIES FACILITY AND ESTIMATES OF THE DISTRIBUTION AND ISOTOPIC COMPOSITIONS OF THESE MINERALS ALONG THE EAST-WEST CROSS DRIFT ALIGNMENT, YUCCA MOUNTAIN, NEVADA

By **James B. Paces, Brian D. Marshall, Joseph F. Whelan, Leonid A. Neymark, and Zell E. Peterman**

DRAFT REPORT

U.S. GEOLOGICAL SURVEY

Open-File Report 98-xxx

Prepared in cooperation with the
NEVADA OPERATIONS OFFICE,
U.S. DEPARTMENT OF ENERGY, under
Interagency Agreement DE-AI08-97NV12033

Denver, Colorado

1998

5. Graphs showing estimates of *A*, simulated infiltration; *B*, fracture density; *C*, fault and shear density; and *D*, hydrogenic-mineral abundance; plotted against distance from the north portal of the Exploratory Studies Facility. .....

6. Graph showing the relation between hydrogenic-mineral abundance and simulated infiltration. .....

7. Graph showing the relation between hydrogenic-mineral abundance in welded units of the Topopah Spring Tuff and the number of faults and shears in the Exploratory Studies Facility. .....

8. Histograms of hydrogenic-mineral abundances in three stratigraphic units of the Topopah Spring Tuff. .....

9. Graph summarizing hydrogenic-mineral abundances in welded tuffs in the Exploratory Studies Facility. .....

10. Histograms showing radiocarbon and uranium-series ages obtained for outer mineral surfaces. .....

11. Graph showing the covariance between initial $^{234}U/^{238}U$ activity ratios and $^{230}Th/U$ ages for calcite and opal deposits. .....

12. Graph showing the distribution of radiocarbon and uranium-series ages for outer surfaces of hydrogenic minerals in the Exploratory Studies Facility. .....

13. Graphs showing variations of $\delta^{87}Sr$ in pore water and initial $^{234}U/^{238}U$ activity ratios in hydrogenic minerals versus vertical distance from the base of the Paintbrush Group nonwelded tuffs. .....

14. Geologic cross section of Yucca Mountain across the potential repository block along the alignment of the East-West Cross Drift. .....

15. Graphs showing the hydrogenic-mineral abundances estimated for the East-West Cross Drift. .....

16. Graphs showing *A*, $\delta^{18}O$ and *B*, $\delta^{13}C$ versus the depth from land surface for latest calcite deposits in the Exploratory Studies Facility. .....

17. Graphs showing estimates of *A*, $\delta^{18}O$; *B*, $\delta^{87}Sr$; and *C*, maximum initial $^{234}U/^{238}U$ activity ratios for hydrogenic minerals in the East-West Cross Drift. .....

18. Graph showing initial $^{234}U/^{238}U$ activity ratios for hydrogenic minerals from the Exploratory Studies Facility plotted against vertical distance from the base of the Paintbrush Group nonwelded tuff. .....

TABLES

1. Calcite and opal abundances in the Exploratory Studies Facility.

2. Summary of calcite and opal abundances in the Exploratory Studies Facility grouped by stratigraphic unit and location. .....

3. Estimates of the abundance of and selected isotopic compositions for calcite and opal in the East-West Cross Drift. .....

DRAFT REPORT

CONVERSION FACTORS AND VERTICAL DATUM

Multiply	By	To Obtain
centimeter (cm)	0.3937	inch
gram (g)	0.03527	ounce
kilometer (km)	0.6214	mile
meter (m)	3.2808	foot
millimeter (mm)	0.03937	inch
millimeter per year	0.03937	inches per year
millimeters per million years (mm/m.y.)	0.03937	inches per million years

Temperature: Degrees Celsius (°C) can be converted to degrees Fahrenheit (°F) by using the formula °F=[1.8(°C)]+32. Degrees Fahrenheit can be converted to degrees Celsius by using the formula °C=(°F-32)/1.8.

Isotope notation: Oxygen-18 (^{18}O), carbon-13 (^{13}C), and strontium-87 (^{87}Sr) are reported using delta (δ) notation in units of parts per thousand (per mil). Delta notation ($\delta^{18}O$, $\delta^{13}C$, or $\delta^{87}Sr$) represents the relative difference between $^{18}O/^{16}O$, $^{13}C/^{12}C$, or $^{87}Sr/^{86}Sr$ measured for a sample and a standard value. The standards are Vienna Standard Mean Ocean Water, VSMOW, for $\delta^{18}O$; Pee Dee belemnite, PDB, for $\delta^{13}C$, and modern ocean water (0.7092) for $\delta^{87}Sr$.

Sea level: In this report, "sea level" refers to the National Geodetic Vertical Datum of 1929 (NGVD of 1929) – a geodetic datum derived from a general adjustment of the first-order level nets of both the United States and Canada, formerly called "Sea Level Datum of 1929."

DRAFT REPORT

SUMMARY OF CALCITE AND OPAL DEPOSITS IN THE EXPLORATORY STUDIES FACILITY AND ESTIMATES OF THE DISTRIBUTION AND ISOTOPIC COMPOSITIONS OF THESE MINERALS ALONG THE EAST-WEST CROSS DRIFT ALIGNMENT, YUCCA MOUNTAIN, NEVADA

By James B. Paces, Brian D. Marshall, Joseph F. Whelan, Leonid A. Neymark, and Zell E. Peterman

Abstract

Low-temperature hydrogenic minerals (predominantly calcite and opal precipitated from water under ambient conditions) in the subsurface at Yucca Mountain, Nevada, represent records of past percolation through the thick unsaturated zone being studied as a potential repository for high-level radioactive waste. The morphology, distribution, abundance, ages, and isotopic compositions of calcite and opal deposits in the Exploratory Studies Facility, an 8-kilometer-long tunnel east of the potential repository block, were summarized. Interpretations of these hydrogenic-mineral data were used along with the mineral data from the Exploratory Studies Facility to estimate the distribution of mineral abundance, $\delta^{18}O$ and $\delta^{87}Sr$ values, and maximum initial $^{234}U/^{238}U$ activity ratios of hydrogenic-mineral deposits expected to be found in the 2.8-kilometer-long East-West Cross Drift after excavation. Factors considered in making these estimates included stratigraphy of the volcanic rocks, structural features, depth from surface, and vertical distance below the base of the Paintbrush Tuff nonwelded unit.

INTRODUCTION

Yucca Mountain, in southern Nevada (fig. 1), is being investigated as a site for a potential geologic repository for high-level radioactive waste. The U.S. Geological Survey (USGS) is conducting site-characterization studies of Yucca Mountain for the U.S. Department of Energy (DOE) under Interagency Agreement DE-AI08-97NV12033. The semiarid environment and a thick [500 to 700 meter (m)] unsaturated zone (UZ) are considered positive attributes for long-term isolation of radionuclides from the environment.

The amount of UZ percolation that may contact waste packages is a critical uncertainty that is being addressed in site characterization. Direct observations or measurements of deep percolation flux have not been made in the potential repository horizon through boreholes or the Exploratory Studies Facility (ESF), an 8-kilometer (km)-long tunnel consisting of a decline (north ramp), main drift, and incline (south ramp). Although percolation flux has not been measured directly, water percolating downward in the past has deposited low-temperature hydrogenic minerals (predominantly calcite and opal deposited under ambient temperatures of less than 50°C) in fracture networks where solutions became oversaturated in these phases. The past percolation record contained in these mineral deposits can be investigated through physical, chemical, and isotopic methods. An understanding of these deposits allows evaluation of the UZ hydrologic response to different climates (Whelan and others, 1994) throughout the late Tertiary and Quaternary periods and a better comprehension of the mechanisms and process of fracture flow through the deep UZ. The interpretations of paleohydrology on the basis of these results are relevant to concepts of both present and future percolation in terms of understanding

the distribution of percolation pathways, general fracture-flow processes, relations between percolation and climate-controlled infiltration, averaged fluxes over geologically relevant periods of time, the degree of equilibrium between matrix and fracture water, and the amount of seepage into open cavities. Although measurements of and interpretations from hydrogenic minerals may not be input directly into conceptual or numerical models of UZ flow (Montazer and Wilson, 1984; Bodvarsson and others, 1997), model results should be consistent with the calcite and opal data. If hydrologic interpretations of the calcite and opal data from the ESF are correct, this generalized conceptualization of UZ mineralization at Yucca Mountain should be capable of describing probable distributions and isotopic compositions of hydrogenic minerals elsewhere within the mountain. Assuming similar geologic conditions at the site in the future, the paleohydrologic information obtained from the minerals can be inferred to represent percolation behavior on a time scale relative to that needed for radioactive waste isolation.

The ESF does not intersect the largely unfaulted structural block immediately to the west that would host the potential repository (fig. 1). Starting in April 1998, the DOE is excavating a drift that will cross this block (East-West Cross Drift; TRW Environmental Safety Systems, Inc., 1998) to obtain more reliable information on potential repository characteristics. The East-West Cross Drift alignment extends southwest from the north bend of the ESF at station 19+92 (1,992 meters from the north portal) at an elevation slightly above the potential repository horizon. It will terminate after about 2.8 km in a structurally complex area formed by multiple splays of the Solitario Canyon Fault on the west side of the potential repository block.

The new drift can be used to test the current understanding of UZ hydrogeologic processes largely on the basis of data from the ESF. Calcite and opal deposits record past percolation through the deep UZ, and their abundance and distribution in the Cross Drift can help determine the hydrogeologic characteristics of the potential repository block. Pre-construction estimates of the distribution and nature of hydrogenic minerals can be compared to data collected after completion of the excavation to evaluate the understanding of the processes contributing to UZ flow and mineral deposition.

Purpose and Scope

The purpose of this report is to summarize the results of ongoing studies of hydrogenic minerals in the UZ, describe concepts of UZ paleohydrology, and to use the mineral data and concepts of UZ flow to estimate the distribution and properties of hydrogenic minerals in the East-West Cross Drift alignment.

The first part of this report summarizes morphology, distribution, geochronology, and isotope geochemistry for calcite and opal deposits in the ESF, as well as strontium isotope ratios for pore waters leached from borehole USW SD-7 core. In the second part of this report, these observations are used to form a mineral-based conceptual model of UZ percolation processes at Yucca Mountain over the past tens of thousands to millions of years to form these minerals. In the final section, the hydrogenic-mineral data and conceptual model are used to estimate the probable distribution and characteristics of hydrogenic minerals in the East-West Cross Drift alignment at 50-m intervals. These estimates are based largely on a stratigraphic framework modified by the presence and location of structural features.

Hydrogeologic Background

Yucca Mountain is in the southwestern Nevada volcanic field (Lipman and others, 1966; Christiansen and others, 1977; Byers and others, 1976, 1989) and is composed of a sequence of thick, welded ash-flow tuffs interlayered with thinner nonwelded air-fall and ash-flow tuffs (fig. 1). Miocene volcanic units at Yucca Mountain (dominantly 13 to 11 million years old; Sawyer and others, 1994) were erupted from calderas to the north (Noble and others, 1968). High-angle normal faults have disrupted the originally flat-lying strata and created a series of north-trending structural blocks rotated so that beds dip 5 to 10 degrees to the east (Scott and Bonk, 1984; Carr and others, 1986).

Rocks of the Paintbrush Group and Calico Hills Formation principally constitute the UZ in the central Yucca Mountain area. These rocks include, in descending order, the Tiva Canyon Tuff, Yucca Mountain Tuff, Pah Canyon Tuff, Topopah Spring Tuff, and the Calico Hills Formation. Both the Tiva Canyon Tuff and Topopah Spring Tuff are thick, tabular, regionally extensive ignimbrites consisting mostly of densely welded quartz latite to high-silica rhyolite. In contrast, the Yucca Mountain Tuff and Pah Canyon Tuff are thin, lenticular, and more localized ignimbrites that are largely nonwelded in the central Yucca Mountain area. The underlying Calico Hills Formation consists mostly of nonwelded and bedded tuffs that have been variously altered (0- to 75-percent replacement) to zeolites (Levy, 1991; Bish and Chipera, 1989; Broxton and others, 1987, 1993).

The tuffs at Yucca Mountain have been further subdivided based on lithologic properties (Buesch and others, 1996). An example of the resulting informal nomenclature (for instance, Tptpul) includes a hierarchy of symbols designed to indicate age (the first symbol, T for Tertiary), group (the second symbol, p for Paintbrush Group), formation (the third symbol, t for the Topopah Spring Tuff), member (the fourth symbol, p for crystal-poor), and zone (the remaining symbols, ul for upper lithophysal). Lithostratigraphic units used in this report are listed in table 1. In addition, the tuffs have been informally grouped into hydrogeologic units based on their physical properties (Montazer and Wilson, 1984; Ortiz and others, 1985). Moderately to densely welded units of the Tiva Canyon and Topopah Spring Tuffs (herein designated as Tpc-welded and Tpt-welded) typically have greater fracture density and fracture permeability relative to nonwelded or partially tuffs. Porosity is also greatly reduced by compaction and welding processes such that the matrix permeability in welded tuffs is small relative to nonwelded tuffs. Nonwelded and partially welded parts of the basal Tiva Canyon Tuff and uppermost Topopah Spring Tuff have been grouped along with the Yucca Mountain and Pah Canyon Tuffs and other interbedded nonwelded tuffs to form the informal Paintbrush Tuff nonwelded (PTn) hydrogeologic unit (Montazer and Wilson, 1984; Moyer and others, 1996). Tables illustrating the correlations among lithostratigraphic, thermal/mechanical, and hydrogeologic units are given elsewhere (Buesch and others, 1996; Rautman and Engstrom, 1996).

The potential repository is located in the lower of the two welded tuffs (Tpt), which are overlain by 25 to more than 100 m of nonwelded, bedded ash-flow tuffs of the PTn in the central Yucca Mountain area (Moyer and others, 1996). The potential repository horizon is 200 to 300 m above the modern water table, which is at an altitude of 730 to 800 m above sea level (Robison, 1984; Tucci and Burkhardt, 1995). The thickness of the unsaturated zone ranges from 500 to 700 m.

Modern average annual precipitation at Yucca Mountain is approximately 170 mm

(Hevesi and others, 1992); however, precipitation has varied greatly during shifts in Pleistocene climate (Spaulding, 1985;Winograd and others, 1992). Mean annual precipitation during pluvial (glacial) climates may have been 2 to 4 times greater than modern interpluvial conditions and mean annual temperatures may have been up to 10°C cooler (Forester and Smith, 1994).

Although precipitation is monitored at several places on Yucca Mountain, infiltration has not been measured directly. Instead, a model of infiltration has been constructed based on moisture measurements in shallow drill holes combined with data on surface characteristics (elevation, slope angle and aspect, thickness of unconsolidated deposits) (A.L. Flint and others, U.S. Geological Survey, written commun., 1996). This model incorporates the concept that areas of greatest infiltration are correlated with higher elevation, north-facing slopes, and thin veneers of surface deposits. Valleys containing thick alluvial deposits are modeled as areas of low infiltration because of their large water-storage capacity, smaller amounts of precipitation at lower elevations, and greater rates of evapotranspiration.

Hydrochemical and isotopic compositions of infiltrating water have been used to demonstrate that the UZ mineral deposits precipitated from water with an infiltration origin (Peterman and others, 1992; Whelan and Stuckless, 1992). These compositions of infiltrating water are strongly affected by interactions with ubiquitous pedogenic calcite and silica present in colluvial veneers over bedrock, alluvial fill in valley bottoms, and pedogenic cements partially to totally filling shallow veins and fractures within the upper few meters of bedrock.

CALCITE AND OPAL DEPOSITS IN THE EXPLORATORY STUDIES FACILITY

Calcite ($CaCO_3$) and opal ($SiO_2 \cdot nH_2O$) are the two most abundant hydrogenic minerals that were formed in the subsurface at Yucca Mountain after emplacement and cooling of the host tuffs (Whelan and Stuckless, 1992; Vaniman, 1993, 1994). They are present as coatings or partial fillings of fracture cavities and lithophysal voids (primary spheroidal vugs) and have not visibly altered the enclosing rock. These hydrogenic minerals are common in the ESF and are superior in quantity and in quality to those preserved in drill core. Delicate crystal textures and spatial relations between the deposits and the host rock cavities are well displayed in ESF exposures. These features either are destroyed during drilling and core recovery or are not found in the limited scale of the sections of core.

Field studies and laboratory analyses of ESF samples have been conducted since December 1995. The following descriptions are a summary of these data and the resulting interpretations. In this report, ESF spatial information is given as linear distances, in meters, measured from the north portal.

General Morphology

Calcite and opal are nonuniformly distributed throughout the welded tuffs of the ESF as thin (commonly less than 10 mm with a maximum of 60 mm) coatings on fractures and lithophysal cavities. Mineral coatings are thickest and most opal-rich on subhorizontal or low-angle fractures and lithophysal cavity floors. Open fractures and other cavities are rare in nonwelded tuffs (PTn); consequently, hydrogenic minerals are sparse, although some beds are locally cemented with calcite and opal.

Hydrogenic-mineral coatings in the UZ are almost entirely on fracture footwalls or cavity floors, in contrast to saturated environments where vein and cavity deposits usually coat all surfaces. Mineralized fractures in the UZ commonly have apertures exceeding several millimeters. Tighter fractures rarely contain hydrogenic minerals, although hairline fractures that open into mineralized fractures or lithophysal cavities are common. Cavities are never completely filled, and mineral high-water marks are absent.

Calcite forms large (millimeter- to centimeter-scale), clear, well-formed (sparry) crystals. Delicate, high-relief crystal habits are common, especially in lithophysal cavities. Thin, tabular to bladed crystals commonly exceed 1 cm in height with widths less than 1 mm. Latest additions of calcite often form at the tips of these bladed crystals forming a distinctive upward-flaring scepter-like cross-section. Bladed forms are less common in fractures, especially where they are steeply dipping. Instead, low-relief, blocky to tabular crystals become the dominant calcite form. Textures and crystal habits are not uniform over broad areas, and calcites in both settings can show a wide range of textures on centimeter-scale surfaces.

Opal typically forms water-clear solid hemispherical bubbles, botryoidal bubbly masses or thin sheets that coat calcite substrates. Small, individual hemispheres are often isolated on otherwise smooth calcite surfaces resulting in the impression of tiny water droplets. Individual bubbles usually show concentric, internal layering on a micrometer or finer scale. Layers of opal that interfinger with calcite at their interface indicate that the two phases grew on an intermittent, but intimate scale. Opal often forms at the tips of calcite blades, either on top of calcite scepter heads, or between the outermost scepter-head calcite layer and the underlying, older blade.

Outermost surfaces of both calcite and opal are smooth with sharp crystal edges and corners. Evidence of corrosion and pitting is absent at most scales of observation. A very small number of calcites may have pitted surfaces when viewed at high magnification; however, pitting may also be the result of crystal growth on a surface contaminated with impurities (opal bubbles). Basal porous zones can be present as scattered patches of higher porosity calcite in a narrow zone between the calcite coatings and the underlying vapor-phase minerals. It is unclear if these textures are related to variations in crystal growth or if they were formed by dissolution of previously formed calcite near the tuff or vapor-phase contact. If the basal porous zones are related to dissolution, it is clear that the same calcite-undersaturated solutions have not affected more recently formed calcite elsewhere in the coating.

Spatial Distribution

The abundance and distribution of macroscopic calcite and opal in the ESF was measured for 30-m intervals typically on 100-m centers resulting in 81 determinations for 78 stations (table 1). Thickness, length, and orientation of the mineral deposits were measured within a 60-cm-wide band centered on a surveying tape stretched along the right rib of the ESF at a height of 1.2 to 1.7 m above the concrete invert (floor). Cross-sectional areas of hydrogenic minerals were determined from these measurements. Sums of these areas are divided by the total surveyed area (30 m by 60 cm less areas covered by ribs, lagging, or muck) to obtain abundances in percent. Local irregularities of the ESF walls, the complex geometry of the mineral coatings, and the accumulation of rock dust on the ESF walls are sources of measurement error.

Results from the 78 surveys ranged from no observed hydrogenic minerals to one that

had 36 deposits yielding a total hydrogenic-mineral abundance of 0.65 percent (table 1, figs. 2 and 3). In general, nonwelded tuffs (PTn) with large matrix permeability and few open fractures or cavities have small hydrogenic-mineral abundances compared to the welded tuffs (Tpc-welded and Tpt-welded). Abundance data for all intervals in welded tuffs (71 surveys) have an arithmetic mean of 0.084 percent; however, the frequency distribution is strongly skewed (fig. 4a). Logarithms (logs) of the mineral percentages are more symmetrically distributed around a mean value of 0.034 percent (fig. 4b). These results indicate that hydrogenic-mineral populations averaged over 30-meter intervals are better represented by lognormal distributions. In the following discussion, log means are used to represent the average mineral abundances when values for multiple survey intervals are given.

Variations along the Exploratory Studies Facility

Abundances of hydrogenic minerals in the shallow parts of the ESF (first 800 m of the ESF north ramp, and last 400 m of the ESF south ramp) are larger than the overall mean (typically 0.050 to 0.20 percent compared to the overall mean of 0.034 percent). Calcite and opal are sparse or absent in nonwelded tuffs (at 200 to 300, 800 to 1,100, and 6,700 m). Progressively along the ESF north ramp and beneath the PTn, mineral abundances increase in the shallow Tpt-welded between ESF surveys at 1,200 and 1,600 m under Azreal Ridge (log mean of 0.14 percent, fig. 3). Abundances decrease substantially in the shallow Tpt-welded lithophysal zones between 1,700 and 2,300 m (0 to 0.016 percent) that may be related to the proximity of the overlying Drill Hole Wash (fig. 2). This is the largest drainage above the ESF and is modeled as a zone of very low infiltration. The exception in this interval is the survey at 2,200 m, which has the largest percentage and number of hydrogenic-mineral deposits. This survey is close to the western splay of the Drill Hole Wash Fault, mapped as a normal fault in contrast to the strike-slip nature of the easterly splay (Day and others, in press). In the ESF, the western splay has an open, brecciated structure, whereas the eastern splay is much tighter, has subhorizontal slickensides, and contains gouge.

Farther on from the Drill Hole Wash Fault in the ESF (fig. 2), mineral abundances increase in the lower parts of the Tpt-welded upper lithophysal and middle nonlithophysal zones between 2,400 and 3,000 m (log mean of 0.065 percent), and are largely restricted to lithophysal cavities. The northern part of the ESF main drift, between 3,100 and 4,800 m, has highly variable mineral abundances ranging from 0.001 to 0.10 percent with a log mean of 0.020 percent. In contrast, the southern part of the ESF main drift, between 4,900 and 5,600 m, has a consistently larger mineral abundance with no zero values and a log mean of 0.071 percent. Similar abundances are found in the south bend between 6,000 and 6,300 m (log mean of 0.079 percent). However, the intervening survey intervals between 5,700 and 5,900 m in the stratigraphically lowest parts of the middle nonlithophysal and uppermost part of the lower lithophysal zones contain few to no hydrogenic-mineral deposits (fig. 3).

The stratigraphic units in the south ramp are structurally more complex because of repetition by faulting. Mineral abundances are generally lowest in survey intervals between 6,400 and 6,900 m, intermediate for intervals 7,100 through 7,500 m, and highest in the last three survey intervals in the near-surface Tpc-welded (fig. 3).

Potential Factors Controlling Mineral Abundance

Several different factors may control the distribution of hydrogenic minerals in the subsurface, including topography, infiltration,

fracture density, fault and shear frequency, and depth. None of these factors have high degrees of correlation with the measured mineral abundances. The current (1998) infiltration model simulates greater infiltration over bedrock areas compared to alluvium-floored valleys (A.L. Flint and others, U.S. Geological Survey, written commun., 1996). Average simulated infiltration rates corresponding to the same 30-m-survey intervals were calculated from the two-dimensional grid cells immediately overlying the trace of the ESF. The greatest amount of infiltration is simulated above the ESF main drift between 3,000 and 6,000 m (fig. 5a). This ESF interval, however, generally contains the lowest average mineral abundances. In contrast, the model simulates negligible infiltration through the alluvium of Drill Hole Wash, which may account for the general lack of hydrogenic minerals in survey intervals from 1,700 through 2,300 m. Specific simulated infiltration values also can be compared directly with the mineral-survey data (Marshall and others, 1998). These data are plotted (fig. 6) in two separate groups corresponding to the two different welded tuffs (Tpc-welded and Tpt-welded). Simulated infiltration and hydrogenic-mineral abundance in the Tpc-welded may be correlated (r^2 value for linear regression = 0.43) based on a limited number (N = 7) of survey intervals. However, mineral abundances in the Tpt-welded show no linear correlation with simulated infiltration (r^2 = 0.009; N = 50, forced through zero). These observations are interpreted to indicate that, if the abundance of calcite and silica are correlated with percolation, other factors besides simulated infiltration likely control UZ percolation beneath the PTn.

Mineral abundances also can be compared to structural features mapped in the ESF (all fracture and fault data are from S.C. Beason, U.S. Bureau of Reclamation, written commun., 1997). The number of fractures per meter is generally low in the ESF north ramp and increases substantially in the ESF main drift in the Tpt-welded middle nonlithophysal zone (fig. 5b). Many of these fractures are stratabound features formed during cooling of the volcanic rock; therefore, they are unlikely to have long-range continuity that would facilitate UZ flow. Hydrogenic-mineral abundances are not correlated with fracture frequency (fig. 5b).

In contrast to fractures, faults and shears may provide long-range connectivity for percolation. Distributions of these structures in the first 6,200 m of the ESF cluster in two areas between about 1,000 and 1,800 m and between about 4,900 and 5,800 m (fig. 5c). These areas also have mineral abundances that are generally greater than the mean value for the ESF (figs. 3 and 5d). Although some major faults are interpreted to be responsible for greater mineral abundances in adjacent areas (the western splay of the Drill Hole Wash Fault and associated ESF survey at 2,200 m being the most notable example), other major faults have no closely related hydrogenic minerals. In spite of the qualitative observations, no correlation exists when mineral-abundance data from the welded units of the Topopah Spring Tuff are plotted against the number of faults and shears in the corresponding ESF intervals (fig 7). Correlation between these parameters may be lacking, in part, because some of the faults may not effectively transmit water. If faults do act as percolation conduits, they may either lack the open space necessary for hydrogenic-mineral deposition, or flow events may be too frequent to allow solutions to become oversaturated in mineral constituents. Mineral deposits associated with faulting also may be offset from mapped fault planes. For example, large mineral abundances are observed in the ESF between 2,200 and 2,230 m although the western splay of the fault intersects the ESF at about 2,240 m. Therefore, a relation, although a complex one,

may exist between faulting, percolation, and mineral deposition.

Stratigraphic Relations

Depth below the surface or below the base of the PTn also may control the abundance of hydrogenic minerals. To evaluate this possibility, 30-m-survey intervals were grouped by host lithology and separated among the ESF north ramp, south ramp, and main drift. Mineral abundances in the two Tpt-welded units (Tptpul in the north ramp and Tptpmn in the northern part of the main drift) with more than 10 surveyed intervals have skewed frequency distributions (fig. 8) similar to the distribution for the whole population (fig. 4). Therefore, log-mean values are the appropriate representation of unit averages. These data are summarized in table 2 and figure 9. Stratigraphic zones of the Tpc-welded have log means of the hydrogenic-mineral abundances ranging from 0.053 to 0.16 percent. The small number of observations, plus the lack of large variation between percentages in the north and south ramps justifies calculating an overall Tpc-welded log mean of 0.094 percent (N = 9). Percentages for welded zones in the Tpt-welded generally have mineral abundances lower than the Tpc-welded mean, although the Tpt-welded crystal-rich nonlithophysal unit in the ESF north ramp area has a log mean of 0.14 (N = 5). The same zone in the ESF south ramp has a lower percentage of 0.028 (N = 4). The Tpt-welded upper lithophysal zone exposed in the ESF north ramp has a small value of 0.014 percent (N = 11) with a large uncertainty because of the scatter of individual surveys. If the values for surveys under Drill Hole Wash (1,800 to 2,300 m) are excluded, the log mean increases to 0.090 percent (N = 4). The same zone exposed in the ESF south ramp has a value of 0.047 percent (N = 6), and a log mean value for both areas (excluding surveys under Drill Hole Wash) is 0.060 percent (N = 10). This latter value is the preferred estimate, in part, because a similar value is obtained if the lithophysal-rich parts of the underlying middle nonlithophysal zone are combined with the ESF north ramp upper lithophysal data (2,400 to 3,300 m). Mineral abundances for the Tpt-welded middle nonlithophysal zone in the ESF main drift are based on the largest number of surveys and have a log-mean value of 0.030 percent (N = 30), although this value varies from 0.020 percent towards the north to 0.071 percent towards the south (fig. 3). The Tpt-welded lower lithophysal zone was exposed only in one survey (5,700 m) and lacked macroscopic calcite or opal.

Preferred estimates of mineral abundances grouped by stratigraphic position (filled symbols, fig. 9) show an apparent decrease with depth in the Tpt-welded; however, substantial overlap exists in uncertainties among the groups. Nevertheless, this relation will be used to infer a first-order variation in subsurface mineral abundance with depth. This variation is supported by depth-dependent changes in the isotopic composition of calcite and opal in the UZ (see "Isotopic Compositions" section).

Geochronology

Radiocarbon and Thorium-230/Uranium Dating of Outer Mineral Surfaces

Deciphering the depositional history of UZ hydrogenic minerals is an important step in understanding paleoflux. Small percentages of modern carbon are present in outer surfaces (generally 0.1 to 0.2 mm thick) of calcite, resulting in ages between 46,000 and 16,000 radiocarbon years before present (fig. 10). Radiocarbon ages are calculated from the measured percent modern carbon values without corrections for past variation of ^{14}C production in the atmosphere. In contrast, thorium-230/uranium ($^{230}Th/U$) ages for microsamples of outermost calcite and opal shown in figure 10 have ages ranging from

490 to 28 thousand years before present (ka). Subsamples as small as 0.1 milligram (mg) from the same growth surface commonly have widely varying ages that indicate a positive correlation to sample size. Thorium-230/U ages less than 100 ka are only obtained for calcite or opal subsamples representing the outermost 0.05 to 0.2 mm of mineral. Preliminary results for an opal surface sampled to depths of only several micrometers yielded an age of only about 9 ka. No systematic age differences were observed between calcite and opal regardless of fracture or lithophysae setting.

Like ^{230}Th/U ages, calculated initial uranium-234/uranium-238 (^{234}U/^{238}U) ratios, indicative of source-water compositions, can vary widely for subsamples of the same surface or layer. The negative correlation between age and initial ^{234}U/^{238}U ratios (fig. 11) would not be expected in a UZ environment that approached steady state hydrologic conditions over the last few million years. Assuming all material in a given subsample was deposited instantaneously with a uniform initial ratio, the observed covariance would require that ^{234}U/^{238}U ratios in percolating water varied monotonically throughout the Quaternary. In contrast, uniform values of initial ^{234}U/^{238}U ratios are observed over the last 500 thousand years in both pedogenic (Paces and others, 1994) and saturated-zone (Ludwig and others, 1992) environments. Causes for a steady change in ^{234}U/^{238}U ratios of UZ percolation over this time period are difficult to conceptualize considering the constancy of recharge and discharge water. Therefore, the assumptions of instantaneous deposition and uniform ^{234}U/^{238}U ratios in individual calcite and opal subsamples may not be valid.

The geochronological data are better explained if mineral growth is gradual and results in nearly continuous deposition of very thin layers at a scale much finer than sampling techniques were able to resolve. This explanation is supported by growth layering on a micrometer or finer scale in both opal and calcite. Under these mineral-growth conditions, even the thinnest subsamples (0.1 to 0.2 mm) represent mechanical mixtures of multiple laminae that have isotope ratios that are intermediate between those characteristic of the oldest and youngest layers present. Ages calculated from both ^{14}C and ^{230}Th/U isotope data (as well as initial ^{234}U/^{238}U ratios) are dependent, in part, on the subsample thickness and can vary substantially at a given stratigraphic depth or from the same depositional surface (fig. 12). If multiple hydrogenic-mineral coatings form over the same depositional time span, the thickest coatings will have the greatest growth rates, the fewest individual laminae in a 0.1- to 0.2-mm-thick subsample, the youngest ages of the finite-thickness subsample, and the youngest resulting ages for the outermost surface. These relations are observed for mineral coatings in the ESF that have the greatest thicknesses on subhorizontal surfaces in the Tpt-welded upper lithophysal and middle nonlithophysal zones. Calcite and opal subsamples from these sites that are deeper in the ESF stratigraphic section (fig. 12 between distances of 3,000 and 6,000 m) also tend to have the youngest ^{230}Th/U ages relative to the thinner deposits in the Tpc-welded.

A model of slow, continuous deposition (Neymark and Paces, 1996; J.B. Paces and others, U.S. Geological Survey, written commun., 1996) results in calculated apparent ^{230}Th/U ages and initial ^{234}U/^{238}U ratios that follow trends approximating the observed data (heavy lines, fig. 11). The large number of analyses that plot to the right of the steeply sloping segments of these lines indicates that the end-member model of continuous deposition through the present day is not completely appropriate for many of the growth surfaces. Cessation of deposition at a given location or short, but finite, depositional hiatuses are likely in the UZ environment.

Nevertheless, a model of continuous deposition can account for (1) the negative correlation between ^{230}Th/U ages and initial ^{234}U/^{238}U ratios (fig. 11), (2) the observed age discordance between isotopic systems with different half-lives (fig. 10), (3) ages approaching, but not reaching, the practical maximum limit of the isotopic clock (for instance, greater than 45 ka for ^{14}C), and (4) the observation of youngest ages from the thinnest, outermost samples.

Subsampling at a greater scale of spatial resolution is required to evaluate this conceptual model. The simplest form of the continuous-deposition model permits present-day deposition of thin veneers of calcite or opal on some of the outermost surfaces; however, the sampling methods used for the ESF analyses have not demonstrated Holocene (younger than 10 ka) mineral growth. If subsample thicknesses could be reduced to a scale of micrometers, rather than hundreds of micrometers, ^{14}C or ^{230}Th/U ages for outer mineral surfaces considerably younger than the 28 ka (^{230}Th/U) or 16 ka (^{14}C) minimum ages observed in ESF minerals might be obtained. Preliminary experiments support this possibility.

Narrow zones related to faults in the northern part of the ESF containing elevated ^{36}Cl/Cl ratios (vertical dashed lines in fig. 12) have been interpreted as fast flow pathways with substantial components of fracture flow younger than 50 years (Fabryka-Martin and others, 1997). The pattern of radiocarbon and ^{230}Th/U ages of hydrogenic minerals does not change in these zones relative to adjacent areas in the ESF or to the ESF south ramp. Many of the sites with elevated ^{36}Cl/Cl ratios, however, do not contain macroscopic calcite or opal, mostly because the sites lack the open space required for mineral deposition. Where hydrogenic minerals are present in or adjacent to these structurally-related zones, no differences in deposition rates, dissolution effects, or isotopic (oxygen, carbon, radiocarbon, strontium, and uranium) compositions are observed. In spite of the coordination of mineral and chlorine sampling efforts, the lack of consistency between these two data sets remains problematic.

Uranium-Lead Dating of Outer Mineral Surfaces and Interior Layers

Opal and chalcedony from outermost surfaces, as well as from interior layers in mineral coatings, have been dated using uranium-lead (U-Pb) methods (^{206}Pb/^{238}U - ^{207}Pb/^{235}U) (Neymark and others, 1997, 1998). Opal U-Pb ages range from 1.0 to about 0.05 million years before present (Ma) for outermost subsamples. These ages are systematically older than ^{230}Th/U ages from the same surfaces with the most noticeable discordance for subsamples with ^{230}Th/U ages greater than 100 ka. The age discordance is caused by the inability to sample discrete episodes of deposition in the finely laminated minerals and differences in the rates of decay for the different radioactive-isotope systems (Neymark and Paces, 1996; J.B. Paces and others, U.S. Geological Survey, written commun., 1996). The discordance between U-Pb and ^{230}Th/U ages are analogous to those between ^{230}Th/U and ^{14}C ages. In both cases, the radioactive-decay system with the longer half-life (U-Pb relative to ^{230}Th/U and ^{230}Th/U relative to ^{14}C) yields more accurate average ages of deposition than the ages in the older ranges of the ^{230}Th/U and ^{14}C systems.

Water-clear opal from interior positions near the base of the mineral coatings has U-Pb ages of 8 to 4 Ma whereas early, translucent-gray chalcedony in basal positions has U-Pb ages between 10 and 9 Ma. Initial ^{234}U/^{238}U activity ratios of 4 to 10 are calculated from measured ^{206}Pb-^{238}U-^{234}U data from opal younger than 1 Ma. These ratios are similar to the range obtained from U-series data for calcite and opal younger than 100 ka.

Ages of different layers in individual mineral coatings from the Tpt-welded indicate uniform rates of deposition over the last 8 million years (m.y.). Four separate samples with multiple U-Pb dated layers indicate average rates of calcite and opal deposition between 0.7 and 4 mm/m.y. (Neymark and others, 1998). Variations in estimated depositional rates are smaller for subsamples from a single site. These rates, based on long-term average deposition of 10- to 20-mm-thick coatings, are consistent with ^{230}Th/U estimates derived from 0.05- to 0.2-mm-thick subsamples of outermost calcite and opal described in the previous section.

In contrast, more complex growth histories are apparent for mineral coatings in the Tpc-welded. Subsamples from several sites in the Tpc-welded dated by U-Pb techniques have ages of millions of years for outermost surfaces (Neymark and others, 1998) compared to ages less than several thousand years typical for outermost mineral surfaces below the PTn. The older ages in the shallower stratigraphic unit may indicate either long periods of nondeposition or dissolution of surface material.

Isotopic Compositions

Isotopic compositions (δ^{18}O, δ^{13}C, δ^{87}Sr, and initial ^{234}U/^{238}U ratios) of calcite and opal deposits in the ESF vary systematically with depth in the UZ as well as with time as indicated by the isotopic ages of the same materials. These variations can be related to flow processes in the UZ at Yucca Mountain and to changes in climate over the last 8 to 10 m.y.

Observed Oxygen and Carbon Isotopes

Oxygen isotope compositions of subsurface calcite, expressed as δ^{18}O, decrease from about 19 ± 2 per mil near the surface to about 16 ± 2 per mil at the depth of the potential repository. Studies by Szabo and Kyser (1990) showed that this trend is consistent with the theoretical fractionation of oxygen between water and precipitating calcite along an average geothermal gradient of 34°C/km. Additional analyses of calcite from core samples (Whelan and others, 1994) confirm this trend.

Unlike δ^{18}O, stable carbon isotopes, expressed as δ^{13}C, show a wide range of compositions that are not correlated with depth in the UZ but appear to be related to the age of the calcite (Whelan and Moscati, 1998). The youngest calcite has δ^{13}C values between about –5 and –9 per mil, whereas the oldest calcite has δ^{13}C of +2 to +10 per mil. Calcite of intermediate age in individual mineral coatings has δ^{13}C values (-4 to +2 per mil) which are generally between the δ^{13}C values of the older and younger materials. These data, combined with U-series and U-Pb-age data, are interpreted as an indication that δ^{13}C is greater in Pliocene (older than about 1.8 million years) calcite compared to younger, Pleistocene calcite. Except for the oldest calcite, the range of observed δ^{13}C values is consistent with a soil-gas carbon dioxide (CO_2) source of dissolved bicarbonate (Szabo and Kyser, 1990; Whelan and others, 1994). However, soil-gas carbon isotope compositions must have changed during the last 6 m.y. from heavier to lighter δ^{13}C values in order to explain the age-dependent variability in the calcite δ^{13}C values.

Observed Strontium Isotopes

Strontium isotopes in the ESF calcite also vary systematically with the relative age of materials within individual hydrogenic-mineral coatings. Youngest calcite subsamples have larger δ^{87}Sr values between 3.81 and 4.93 per mil whereas older calcite has smaller δ^{87}Sr values (0.42 to 3.95 per mil), although they overlap with the lower end of the range for younger materials. The δ^{87}Sr values in the youngest calcite are similar

to those of pedogenic calcite (Marshall and Mahan, 1994); however, this similarity may be coincidental because, in general, the $\delta^{87}Sr$ calcite values reflect limited water-rock interaction in the overlying volcanic section (Marshall and others, in press). Smaller $\delta^{87}Sr$ values in older ESF calcites are best explained by a model of Sr exchange between fluid and vitric tuff in the PTn during percolation (Marshall and others, in press). Relatively large ratios of rubidium (Rb) to Sr in the nonwelded tuffs have caused the $\delta^{87}Sr$ values to increase over the last 12 m.y. The gradual increase in $\delta^{87}Sr$ in the PTn with time is recorded in the early-to-late-formed ESF calcite, although local equilibrium with the host rocks was not attained.

In addition to hydrogenic minerals, the $\delta^{87}Sr$ values of pore water (or its water-soluble salts) extracted from core obtained from a 250-m-deep borehole (USW SD-7, fig. 1) vary systematically with depth (Marshall and others, in press) showing the largest change in $\delta^{87}Sr$ in the PTn (fig. 13a). The average $\delta^{87}Sr$ of pore water in the Tpc-welded is 3.67 whereas the underlying Tpt-welded has pore water values averaging 4.65. Although the compositional shift is initiated within the basal Tpc-welded, most of the change occurs in the nonwelded tuffs of the PTn. The depth-dependent change in $\delta^{87}Sr$ is the result of progressive water-rock interaction as water passes through the matrix of the more permeable and chemically reactive nonwelded vitric tuff of the PTn (Marshall and others, in press).

Observed Initial $^{234}U/^{238}U$ Ratios

Calculated initial $^{234}U/^{238}U$ ratios, representing the isotopic composition of percolating waters at the time of mineral deposition, also display a pronounced shift between welded tuffs above and below the PTn (fig. 13b). Calcite and opal in the Tpc-welded and PTn have low initial $^{234}U/^{238}U$ activity ratios (1 to 2) that are typical of calcite and opal in the soil environment, whereas the underlying Tpt-welded contains minerals with larger values up to 9.6. Unlike $\delta^{87}Sr$ values, the increase in initial $^{234}U/^{238}U$ ratios occurs below the base of the PTn and, therefore, is not likely caused by the same processes of water-rock interaction in the PTn. As with $^{230}Th/U$ ages, initial $^{234}U/^{238}U$ ratios vary widely for subsamples from the same growth surface. Some of this variation may be the consequence of variable subsample thickness; thicker mineral coatings in the Tpt-welded allow better sampling resolution relative to thinner coatings higher in the section (Tpc-welded). However, this explanation probably cannot account for the absence of minerals with elevated initial $^{234}U/^{238}U$ ratios in the shallow parts of the UZ.

Perched water at Yucca Mountain is capable of attaining similarly elevated $^{234}U/^{238}U$ activity ratios up to 7.6 by mechanisms that preferentially incorporate ^{234}U into solution relative to ^{238}U as percolation moves along fracture flow paths (Paces and others, 1998). These mechanisms (Gascoyne, 1992) include preferential leaching of ^{234}U from radiation-damaged lattice sites (Szilard-Chalmers effect), radiation-induced oxidation of ^{234}U leading to a more soluble ^{234}U-uranyl ion, and alpha-recoil of ^{234}Th from crystal surfaces. The amount of excess ^{234}U preferentially incorporated into migrating solutions is dependent on the mass of U available along flow paths, water-rock ratios, flow-path length, time between flow events in the UZ, and the amount of bulk-rock dissolution. Some combination of these factors results in larger $^{234}U/^{238}U$ ratios in fracture waters below the PTn compared to values in or above the PTn.

The elevated $^{234}U/^{238}U$ values in perched water and initial ratios of hydrogenic minerals at Yucca Mountain appear to be unique in the region. Although many of the volcanic rock

types and UZ thicknesses are similar, perched seeps and springs draining highland areas have smaller activity ratios (less than 4.0; Paces and others, 1998). Therefore, the elevated $^{234}U/^{238}U$ values at Yucca Mountain most likely are caused by low fracture fluxes in the deep UZ relative to recharge areas in the volcanic highlands to the north. Percolation flux in the shallow units may be large enough to prevent accumulation of ^{234}U on flow-path surfaces, thus allowing percolating solutions to retain the $^{234}U/^{238}U$ signatures acquired in the soil zone. In contrast, percolation flux in the Tpt-welded may be small enough to allow ^{234}U to build up on mineral surfaces so that it is not as overwhelmed by the dissolved ^{238}U acquired from the infiltration source or from rock dissolution in the PTn.

MINERAL-BASED IMPLICATIONS FOR UNSATURATED-ZONE PALEOHYDROLOGY

Hydrogenic minerals in the UZ formed over time from downward-migrating water and therefore contain spatial and temporal information concerning the processes of flow in fractures. In this section, interpretations of the data discussed in the first section of the report are used to gain insight into hydrologic mechanisms responsible for mineral deposits, the relations between climate and deep UZ hydrologic response, and variations in flux due to site hydrostratigraphy. Mineral textures and chemical compositions are used to support interactions between downward-migrating water and upward-migrating air in open cavities. Textural differences of coatings on steep- and shallow-dipping surfaces also suggest that subhorizontal sites may be the most important areas of water-air exchange. The absence of hydrogenic minerals in many open cavities indicates that these sites have remained isolated from fracture flow. Uniform long-term deposition rates obtained from mineral coatings below the PTn indicate that the deep UZ may be buffered from variations in infiltration caused by shifts in Tertiary and Quaternary climate. These mineral-based hydrologic implications are compared to various aspects of a previous conceptual model of UZ flow (Montazer and Wilson, 1984) and support the conclusion of the PTn playing an important role in diverting or moderating infiltration flux as well as the concept of negative flux by removal of upward-migrating water vapor (and CO_2).

The distribution and textures of the hydrogenic minerals in fractures and cavities reflect depositional processes associated with UZ flow. Textural evidence indicates that mineral deposition in and above the potential repository horizon occurs under unsaturated hydrologic conditions rather than in zones of local water perching. Open space is needed for deposition, and the restriction of hydrogenic minerals to fracture footwalls and cavity floors indicates the predominance of gravitational rather than capillary forces on solutions that percolate through fracture networks. Bladed calcite textures, and the common location of opal at sites of highest relief on substrate surfaces, indicate that mineral growth occurs preferentially on crystal tips and edges rather than on faces. Therefore, percolating solutions commonly become oversaturated in mineral components not in areas near the base of the coatings where water might concentrate, but at crystal extremities were the greatest gas flux may occur.

A depositional scenario consistent with observed textures involves water moving down connected fractures as thin sheets or films (Tokunaga and Wan, 1997). Subhorizontal cavity surfaces may be particularly effective at slowing vertical fracture flow. Confined flow may spread laterally at these sites resulting in large surface areas for evaporation and vapor removal. Continuous removal of small

quantities of water vapor and CO_2 under conditions of low percolation flux is likely to result in supersaturation and precipitation of hydrogenic minerals. An evaporation origin for opal is consistent with similarities between U/SiO_2 ratios observed in opal [20 to 300 micrograms per gram (μg/g) U and about 95 weight percent SiO_2] and ground water [0.5 to 5 nanograms per gram (ng/g) U and 30 to 70 mg/L SiO_2]. Pore water and perched water with these SiO_2 concentrations are close to saturation with respect to amorphous silica. Therefore, as small amounts of water slowly evaporate, uranium and SiO_2 are incorporated into opal in approximately the same proportions as in the water. These concentrations also imply that the uranium distribution coefficient (D_U) between concentrations in opal ($[U]_{solid}$) and water ($[U]_{water}$), or $D_U = [U]_{solid} / [U]_{water}$, ranges between 10^4 and 10^6. Experiments involving laboratory precipitation of silica gel from a water with known uranium concentrations resulted in substantially lower D_U values between 10^2 and 10^3 (Zielinski, 1980). If the experimental conditions are appropriate for those in the UZ at Yucca Mountain, opal precipitating from water with the U concentrations of 0.5 to 5 ng/g would have uranium concentrations of only 0.05 to 5 μg/g. The larger values measured in opals may indicate that solutions become supersatured in silica by evaporation at the site of deposition.

Many of the lithophysae and fracture cavities in the welded tuffs do not contain hydrogenic minerals, and open spaces lacking calcite and opal are commonly adjacent to sites with thick mineral coatings. Several reasons may cause this extremely heterogeneous spatial distribution. Unmineralized sites may simply represent cavities along flowpaths that permit water to gain ingress, but do not allow the loss of vapor. This condition may exist where hairline fractures remained full of water so that percolation can drip in without allowing removal of gases along the same path. Although this constrictive geometry is possible, it seems unlikely that such pathways would allow substantial or rapid flux. The absence of calcite or opal deposits in cavities is more likely caused by the absence of percolation into the openings. If water had episodically flowed through these sites, thin films and droplets would remain after the main percolation pulse. These solutions would not have remained undersaturated with respect to calcite and opal as evaporation occurred. Consequences of fracture flow are likely to include the gradual development, although extremely slowly, of hydrogenic-mineral coatings on these surfaces. Therefore, it is reasonable to conclude that open fractures or cavities lacking calcite and opal deposits have not had substantial percolation since the emplacement of the tuffs.

Uniform rates of mineral deposition over the last 8 m.y. indicate that hydrologic conditions in the potential repository horizon have remained relatively constant despite gradual, but major, changes in climate during this time period. The correlation of $\delta^{13}C$ with U-Pb age (Whelan and Moscati, 1998) most likely documents an evolution of plant communities reflecting a shift from a climate favoring C_4-type plants (grasses) in the Miocene to one favoring predominantly C_3 plants (shrubs and trees) in the Quaternary. Regional studies (Smith, 1984; Winograd and others, 1985; Larson and others, 1991; Thompson, 1991) support the concept of a major shift in climate from wetter, milder conditions in the Pliocene to drier conditions with greater seasonal extremes in the Pleistocene. Climate fluctuations during the Pleistocene might be expected to result in nonuniform periods of mineral formation. If deposition occurs predominantly during either wetter pluvial or drier interpluvial conditions, mineral ages would be clustered, reflecting major periods of mineral formation. The

absence of clustered ^{230}Th/U ages from 400 to 50 ka (fig. 10), may indicate that climate changes do not result in substantial variations in mineral growth and associated percolation in the deep UZ during middle and late Quaternary pluvial and interpluvial cycles. Although additional dating efforts at an increased scale of spatial resolution (microbeam analysis, micro-digestion) are needed to better resolve the true distribution of depositional ages, broad clusters of ages would be expected as long as the duration of depositional episodes is subequal to that of nondeposition. If the apparent uniform distribution of ages is accurate, it represents evidence that variations in meteoric precipitation and associated infiltration are not translated directly downward from the surface to the potential repository depth as percolation.

Hydrogenic-mineral and pore-water data indicate that the permeable, nonwelded units of the PTn have a major effect on UZ flow. Differences in morphologies, ages, and initial ^{234}U/^{238}U activity ratios between hydrogenic minerals in the Tpc-welded and Tpt-welded indicate that changes in percolation processes or rates coincide with the presence of the PTn. The lack of correlation between the distribution of mineral deposits and simulated infiltration (figs. 5 and 6) may also indicate that the PTn modifies vertical flow. The pore water δ^{87}Sr data indicate that percolation entering the PTn is slowed enough to allow water-rock interactions with the porous vitric matrix of this unit (Marshall and others, in press). In addition, the contrast between maximum initial ^{234}U/^{238}U ratios in the Tpc-welded and Tpt-welded is possibly explained by differences in total fracture flux between the shallower and deeper units separated by the PTn. The absence of obvious correlations between mineral records in the Tpt-welded and climate variations on both longer and shorter time scales further supports the concept that percolation in the deep UZ is moderated by flow through the contrasting hydrogeologic units.

Many of the mineral-based implications for UZ paleohydrology are consistent with concepts of UZ flow proposed by Montazer and Wilson (1984) and are illustrated in figure 14. These authors noted the strong potential for lateral flow through the PTn because of the eastward dip and the much larger lateral relative to vertical conductivity in nonwelded tuffs. The higher effective porosity of the PTn relative to welded tuffs also creates a large storage capacity for recharge from the Tpc-welded. Once imbibed, percolation can flow eastward through the PTn to areas of structural disruption where more focused vertical flow can resume. A capillary barrier at the contact between the PTn and the underlying Tpt-welded may limit the amount of water that is transferred to the fractures in the deep UZ (Montazer and Wilson, 1984).

Montazer and Wilson (1984) also recognized the importance of upward transport of water through convection of vapor-saturated air. The thick UZ allows large thermal gradients to be established, and the fractured nature of the welded tuffs provides numerous air pathways. The network of unmineralized fractures may allow an effective transfer of upwardly migrating air, but not permit downward percolation. Using geothermal heat-flux data and modeling techniques presented in Sass and Lachenbruch (1982), Montazer and Wilson (1984) calculated a large negative (upward) flux of vapor-saturated air in the Tpt-welded. Substantial water-vapor loss through convection, although at slow rates, is consistent with the textural data discussed earlier in this section.

Percolation in fractures of the Tpt-welded may be further reduced by water-air interactions in the upper lithophysal zone. Mineralized lithophysae in this zone contain the thickest hydrogenic deposits observed in

the ESF. Cavities intersected by fracture pathways slow percolation by allowing water to spread laterally within the opening and by permitting a large water-air interface for enhancing evaporation. This process is probably responsible for the contrast in textures between thin coatings of blocky calcite on steep fracture surfaces and thick coatings of elongated calcite blades on shallow dipping fractures and lithophysae floors. This process may be one of the main mechanisms causing the observed decrease in mineral abundances with depth below the PTn (fig. 9).

Interpretations of hydrogenic-mineral data discussed in this section support the concept of reduced percolation in areas of the Tpt-welded overlain by the PTn relative to net infiltration and shallow percolation above the PTn. Both lateral diversion of percolation in the PTn to areas of structural disruption and upward fluxes of water-saturated air are possible mechanisms that could result in less percolation through the potential repository horizon.

ESTIMATES OF CALCITE AND OPAL DEPOSITS IN THE EAST-WEST CROSS DRIFT ALIGNMENT

The data and interpretations developed from the study of hydrogenic minerals in the ESF can be used to estimate the probable distribution and isotopic variability of hydrogenic minerals elsewhere in Yucca Mountain. Estimates of the mineral distribution and characteristics along the East-West Cross Drift alignment (fig. 1) can be compared to actual data measured after the drift is excavated. In this report, probable mineral abundance and isotopic compositions are estimated for 50-m intervals along the alignment (table 3) and represent average values over the intervals rather than values expected at a given site.

Probable Mineral Distribution

Estimates of hydrogenic-mineral abundances for the East-West Cross Drift (table 3, fig. 15) are primarily based on values determined for the different Tpt-welded subunits where the PTn is present (table 1) and on Tpc-welded values where the PTn is absent in Solitario Canyon. Additional considerations for developing the estimates are based on (1) the proximity of the ESF to the northeastern part of the East-West Cross Drift and the assumption that values would be similar, (2) the effects of faults, and (3) the lack of information available for some units. Distances in the East-West Cross Drift are given in meters with a starting point (zero) at the centerline of the ESF in the north ramp at ESF station 19+92, 1,992 m from the reference point at the north portal.

The first 200 m of the East-West Cross Drift underlie Drill Hole Wash, and the host rock is the upper lithophysal zone (Tptpul) of the Tpt-welded. Estimated hydrogenic-mineral abundances in the East-West Cross Drift at 0 and 50 m are based on the ESF survey at 2,000 m. The ESF mineral abundances are small beneath Drill Hole Wash except for the ESF survey at 2,200 m that is close to the western splay of the Drill Hole Wash fault. Therefore, the log means for ESF surveys 1,700 through 2,100 m are used to estimate an abundance of 0.0019 percent at 100 and 200 m in the East-West Cross Drift; the Drill Hole Wash fault crosses the East-West Cross Drift between these stations. The value for ESF survey 2,200 m (0.65 percent) is used to estimate the abundance at station 150 m assuming similar geometry and percolation characteristics as in the ESF, approximately 170 m to the northwest.

The log-mean percentage of hydrogenic minerals in the upper lithophysal zone away from Drill Hole Wash is assumed to be representative of this unit elsewhere and is used to estimate the probable abundance for

most of the intervals in the East-West Cross Drift between 250 and 1,000 m. The northern end of the Ghost Dance Fault is projected to intersect the East-West Cross Drift between 450 and 500 m. This fault is not expected to cause much change in hydrogenic-mineral abundances in the East-West Cross Drift because of the very small vertical displacement of the overlying PTn and the small percentage of hydrogenic minerals in or adjacent to the fault in ESF exposures several kilometers to the south. At about 760 m, the East-West Cross Drift will cross above the main drift of the ESF. Percentages for ESF surveys 3,000, 3,100, and 3,200 m are used to estimate East-West Cross Drift values at 700, 750 and 800 m, respectively, because of the proximity of the Cross Drift to the ESF. The East-West Cross Drift will intersect the northwest-trending Sundance Fault between 1,070 and 1,100 m. The effects of this fault on mineral abundance are not expected to be important, because the strike-slip, compressional nature of faults with this orientation have limited hydraulic conductivity compared to north-south, extensional faults (Kolm and Downey, 1994; Faunt, 1997). In addition, no obvious differences in mineral abundances were observed in or on either side of the Sundance fault in the ESF (3,600 to 3,700 m) (fig. 2); therefore, log means for the Tpt-welded upper lithophysal zone (Tptpul) and middle nonlithophysal zone (Tptpmn) are used to estimate values for the East-West Cross Drift at 1,050 and 1,100 m, respectively.

The East-West Cross Drift alignment between 1,150 and 2,250 m is characterized by increasing depth below the base of the PTn and the absence of faults. The log-mean mineral abundances of the Tpt-welded middle nonlithophysal zone in the ESF (Tptpmn, table 2) are used to estimate the values in the East-West Cross Drift interval of 1,150 to 1,650 m. The gradational contact of this zone with the underlying lower lithophysal zone (Tptpll) is at about 1,650 m. The lower lithophysal zone was present in only one survey interval in the ESF (5,800 m) and no hydrogenic minerals were observed. Adjacent survey intervals in the lowermost parts of the middle nonlithophysal zone in the ESF also had very small mineral abundances (0.0019 and 0.000 percent) (table 1). Assigning a zero value to the lower lithophysal zone on the basis of a single ESF survey interval is unrealistic due to the insufficient sample population. The small abundances observed for this ESF interval, as well as the general decrease in mineral abundance with stratigraphic depth (filled circles, fig. 9), is the basis for assigning a small abundance value to the lower lithophysal zone in the East-West Cross Drift. Estimates of hydrogenic-mineral abundances for the East-West Cross Drift between 1,700 and 2,250 m are based on the log mean value for the middle nonlithophysal zone (Tptpmn) in the ESF multiplied by an arbitrary factor of one-third. The resulting value of 0.010 percent is consistent with the pattern of decreasing abundance with depth in the Tpt-welded (fig. 9).

Nonwelded units of the PTn crop out on the west side of Yucca Mountain about halfway up the eastern side of Solitario Canyon (fig. 14). This outcrop corresponds to the interval between 2,260 to 2,360 m in the East-West Cross Drift beyond which the PTn is absent in the overlying rock mass. The contact between lower lithophysal zone (Tptpll) and lower nonlithophysal zone (Tptpln) is also at about 2,360 m. The lower nonlithophysal zone is not exposed in the ESF; however, the absence of overlying PTn is probably more important than stratigraphic depth in controlling UZ flux through this interval. Because the PTn is not present to influence vertical flow, deep percolation is probably greater in this interval (2,350 to 2,450 m) of the East-West Cross Drift. As a result, mineral abundances in this unit could

be similar to those in the welded tuffs overlying the PTn. Therefore, the log mean Tpc-welded mineral abundance of 0.094 is used to estimate abundances between 2,350 and 2,450 m in the East-West Cross Drift. A value intermediate between the log mean Tpc-welded value and the one used to estimate the abundance at 2,250 m is used for the transitional interval at 2,300 m.

The remainder of the East-West Cross Drift will intersect a complex series of fault blocks associated with the north-trending Solitario Canyon Fault. These structural complexities plus a paucity of borehole stratigraphic control result in greater uncertainties in the geologic framework of this part of the alignment (left undifferentiated in fig. 14) relative to the main Yucca Mountain block. The main splay of the Solitario Canyon Fault is a block-bounding normal fault associated with a major drainage west of the crest of Yucca Mountain (figs. 1 and 14). These factors may contribute to a larger percolation flux in this area. The Tpc-welded log-mean percentage multiplied by an arbitrary factor of 3 is used to estimate mineral abundances for intervals associated with the Solitario Canyon Fault (2,500, 2,550, and 2,650 m). If thicker deposits of alluvium substantially decrease infiltration (A.L. Flint and others, U.S. Geological Survey, written commun., 1996), as is possible beneath Drill Hole Wash, stations west of about 2,600 m may have much smaller mineral abundances than listed in table 3. The station at 2,600 m occurs in a down-dropped wedge containing both Tpc-welded and PTn overlying the Tpt-welded (Tptpul at the alignment level). The log mean of the Tptpul from the ESF was used as an estimate of the mineral abundance at this station (table 3); however, the nearby, potentially-transmissive faults and thicker surface deposits may have a substantial effect within this fault wedge. The station at 2,700 m intersects the Tptpmn within a thin upthrown structural block where the PTn has been removed. The log mean abundance value for Tpc-welded was used to estimate mineral abundance at this station, although the same effects from faulting and surface deposits described for station 2,600 may occur. The final two stations at 2,750 and 2,800 m are wholly or partly in bedded tuffs of the PTn. Mineral abundances are expected to be small because of the assumed lack of open cavities. Percentages ranged from zero to 0.013 in five PTn intervals measured in the ESF (table 2). Therefore, the two stations in the PTn in the East-West Cross Drift are expected to have less than 0.005 percent hydrogenic-mineral abundances.

Although estimated uncertainties are large, the expected trend is one of decreasing mineral abundance with increasing distance westward in the Cross Drift where the PTn is present (fig. 15). This trend is reversed in the last 450 m of the drift where the general absence of the PTn and the presence of major structural flow paths are expected to increase deep percolation flux and associated mineral abundance.

Actual mineral abundances in the East-West Cross Drift should clarify the effect of the PTn on the diversion of infiltration. Most of the Cross Drift will underlie surfaces with only veneers of unconsolidated soil and colluvium rather than thick alluvium. Furthermore, surface elevations generally increase with increasing distance westward along the drift. Both of these factors support an increase in simulated infiltration (A.L. Flint and others, U.S. Geological Survey, written commun., 1996) towards the west with a maximum infiltration along the crest of Yucca Mountain between 1,700 and 2,100 m in the East-West Cross Drift. If the infiltration model can be used to estimate deep percolation, abundances of hydrogenic minerals should increase as the Cross Drift proceeds to the southwest, contrary to the

estimates presented here for the part of the Cross Drift overlain by the PTn.

Estimated Ages of Hydrogenic Minerals

Location-specific ages for hydrogenic minerals in the East-West Cross Drift are not estimated in this report because of the complex relations between growth rates, subsample thickness, uneven deposition on sample surfaces, and variable growth histories (see "Geochronology" section). However, in a general sense, ages of hydrogenic minerals throughout parts of the East-West Cross Drift overlain by the PTn are expected to be similar to those measured in Tpt-welded units in the ESF. If subsampling of these deposits uses the same methods as in the ESF, similar ^{14}C, $^{230}Th/U$ and U-Pb ages are expected (fig. 10). Youngest ^{14}C ages of calcite outer surfaces are expected to range from 20 to 15 ka with most of the determinations between 45 and 25 ka. The same youngest surfaces should have youngest $^{230}Th/U$ ages between 50 and 25 ka with older ages (500 to 100 ka) for most of the determinations. Dating of outermost surfaces by U-Pb should give a range of ages that is systematically older than the $^{230}Th/U$ with most ages between 1,000 and 100 ka. Ages for interior parts of mineral coatings should have the same range as those observed in ESF coatings (8 to 4 Ma for basal layers).

The PTn is generally absent in the westernmost 450 meters of the East-West Cross Drift. Mineral deposits in this part of the Cross Drift are more likely to show the effects of variable hydrologic responses to climate. Apparent ages of outer mineral surfaces may be older than those in the potential repository block to the east for the same reasons that minerals in the Tpc-welded have older apparent ages relative to the Tpt-welded. However, if the larger volumes of percolation expected along the Solitario Canyon Fault result in thick deposits of calcite and opal in adjacent cavities, ages as young or younger than those in the ESF may be obtained.

Estimated Isotopic Compositions

Oxygen and Carbon Isotope Estimates

A negative correlation of $\delta^{18}O$ values in calcite with depth below land surface was observed in core samples (Szabo and Kyser, 1990; Whelan and others, 1994). Extensive sample collections from the ESF, although limited in depth range compared to drill-core samples, confirm the trend of decreasing $\delta^{18}O$ with depth (fig. 16a). The paucity of data in the range of 100 to 150 m is due to the overall absence of hydrogenic minerals in the PTn for this interval. Although the calcite $\delta^{18}O$ values may range more than 2 per mil at any given depth, values generally decrease from almost 20 per mil in the shallow Tpc-welded to values close to 17 per mil in the deepest exposures of Tpt-welded in the ESF. A linear regression of these data has a slope of –0.0104 per mil/m, an intercept of 19.9 per mil, and a correlation coefficient (r^2) of 0.7 (fig. 16a). A 1-per mil error envelope on either side of this line includes most of the data points.

The relation between depth and $\delta^{18}O$ observed in ESF calcite forms the basis for estimating probable oxygen isotope compositions of calcite in the East-West Cross Drift (table 3). Depth from the surface along the Cross Drift alignment ranges from about 180 to 370 m. Based on the trend shown in figure 16a, calcite $\delta^{18}O$ in the East-West Cross Drift will range from about 18 per mil in the eastern and western parts of the drift to a low value of about 16 per mil under Yucca Crest (fig. 17a).

A clear relation between depth and $\delta^{13}C$ in late-formed calcite is less compelling than the relation with $\delta^{18}O$ (fig. 16). Although a linear regression of the data indicates a slight

$\delta^{13}C$ decrease with depth, the correlation coefficient (r^2) is only 0.2. The linear trend is defined by a relatively small number of analyses in the deepest parts of the ESF that have $\delta^{13}C$ values between –7 and –8 per mil. The same range of $\delta^{13}C$ (–5 to –6 per mil) in the shallow Tpc-welded calcite is encompassed in the range at greater depth in the Tpt-welded. Decreasing $\delta^{13}C$ values with depth are not expected in the Cross Drift because decreases in $\delta^{13}C$ values of percolating water caused by calcite precipitation will be offset by the increase in $\delta^{13}C$ caused by CO_2 evasion. An additional complication in interpreting these data is the increase in $\delta^{13}C$ for older calcite (Whelan and Moscati, in press). Although the data plotted in figure 16b represent subsamples of outermost calcite, most of these are not dated isotopically. Therefore, some of the values between –5 and –6 per mil observed in the Tpt-welded calcites may represent older materials. Because of the ambiguities in $\delta^{13}C$ versus depth relations, location-specific estimates for hydrogenic minerals in the East-West Cross Drift are not presented.

Strontium Isotope Estimates

Strontium isotope compositions of calcite can indicate the source of the strontium, assuming the range of compositions in possible source materials is known. Although $\delta^{87}Sr$ values of thin calcite coatings obtained from drill core indicated a surficial source for the strontium (Peterman and others, 1992), this explanation cannot account for the wider range of compositions observed in thick calcite coatings from the ESF. The thicker coatings allowed more detailed sampling that revealed a general microstratigraphic variation in $\delta^{87}Sr$. With increasing depth into the coating, the $\delta^{87}Sr$ values decrease (Marshall and others, in press).

A water-rock reaction model for pore-water strontium data from borehole USW SD-7 (Marshall and others, in press) can explain the $\delta^{87}Sr$ variations of ESF calcite. The strontium isotope compositions of pore water change systematically with depth, and the upper and lower contacts of the PTn unit are marked by changes in slope of the $\delta^{87}Sr$ depth profile (fig. 13). The $\delta^{87}Sr$ values in pore water can be explained by water-rock interaction in the PTn. The nonwelded tuffs are more reactive than the welded tuffs because of their predominantly vitric constituents (compared to the quartz and alkali feldspar matrix of devitrified welded tuffs) and their much greater porosity. Using the strontium concentrations and $\delta^{87}Sr$ values of the whole-rock core, Marshall and others (in press) calculated a downhole cumulative rock $\delta^{87}Sr$ that closely approximates the pore-water data, at least below the PTn. Then, by using the known variation in $\delta^{87}Sr$ in the rocks over time (because of in-situ radioactive decay of ^{87}Rb), an estimated pore-water $\delta^{87}Sr$ value may be calculated for any depth in the Tpt-welded at any time in the past. At the depth of the ESF, this model is used to estimate a probable range for the pore water $\delta^{87}Sr$ values that closely approximate the range measured in ESF calcite. Also, ages predicted by this model are in general agreement with U-Pb dates determined for older parts of the mineral coatings (Neymark and others, in press). Therefore, the strontium contained in ESF calcite is indicative of slowly percolating water that is closely related to, but not necessarily in local equilibrium with, matrix pore water.

Using the model developed for borehole USW SD-7, a linear regression of pore-water $\delta^{87}Sr$ and depth is $\delta^{87}Sr = 0.00172 * z + 4.55$, where z is the depth in meters below the base of the PTn (fig. 13). This equation approximates the $\delta^{87}Sr$ values of latest calcite from the ESF. Deviations from the conceptual model and incorporation of older calcite in a subsample will result in smaller measured $\delta^{87}Sr$ values. Therefore, the model will be

used to estimate the probable maximum $\delta^{87}Sr$ values of calcite in the East-West Cross Drift. Relations between $\delta^{87}Sr$ and depth developed from a single borehole may have limited application elsewhere because of variations in infiltration rates and PTn thickness that result in variable residence times of water in the nonwelded tuffs. Increased infiltration and reduced PTn thickness both tend to decrease pore-water residence time in the PTn and thus decrease the shift in $\delta^{87}Sr$ from infiltrating soil-zone compositions.

Where the PTn is absent because of erosion or faulting, the distributions of $\delta^{87}Sr$ values for soil calcite can be used directly to estimate the $\delta^{87}Sr$ in calcite at depth. Thus, in the absence of the PTn, the $\delta^{87}Sr$ of percolating water will be only slightly modified by water-rock interaction.

The estimates of $\delta^{87}Sr$ values for outermost calcite in the East-West Cross Drift are presented in table 3 and in figure 17b. The PTn is present over the first 2,300 m of the Cross Drift alignment, and the distance between the Cross Drift and the base of the overlying PTn generally increases to the southwest. Delta ^{87}Sr is estimated to increase from +4.69 per mil at the beginning of the Cross Drift to +4.99 per mil at a distance of 2,300 m. This range is within the ±0.5 per mil error of the estimates. Thus, the $\delta^{87}Sr$ values of latest calcite sampled from the Cross Drift are expected to be similar to those from the ESF and the likely variation is small. Beginning at about 2,300 m, the PTn is absent from the overlying section. The $\delta^{87}Sr$ of calcite will then reflect the $\delta^{87}Sr$ values in the overlying soils, with little additional variation caused by water-rock interaction. Where the soil cover is thin and lacks well-developed calcrete, the soil $\delta^{87}Sr$ values should be similar to the value of +3.4 ± 1.1 per mil determined for calcite from thin soils and bedrock coatings (Marshall and Mahan, 1994). Where the overlying soil becomes thicker in Solitario Canyon (between 2,600 and 2,800 m), strontium from calcrete may dominate the isotopic composition at depth. A larger $\delta^{87}Sr$ mean value of +4.4 ± 0.8 per mil characterizes calcite from well-developed calcretes (Marshall and Mahan, 1994). Error estimates in table 3 are intended to include the range of expected values produced by the models presented.

Initial $^{234}U/^{238}U$ Ratio Estimates

Maximum initial $^{234}U/^{238}U$ activity ratios observed in ESF hydrogenic minerals increase with depth below the PTn (fig. 18) ranging from about 2.2 within 10 m of the base of the PTn to between 7.5 and 9.6 in the deepest parts of the Tpt-welded exposed in the ESF (about 150 m below the base of the PTn). As discussed in the section on observed initial $^{234}U/^{238}U$ ratios, the most likely cause for this depth-dependent shift is the decrease in the ratio between percolation volumes and increasing UZ flow-path lengths in fractures below the PTn. Analyses with maximum initial $^{234}U/^{238}U$ ratios at various levels in the Tpt-welded section were selected as the values that most closely reflect maximum isotopic compositions of the original fracture water. Depths between 0 and about 60 m below the base of the PTn are not well represented in the ESF data set. In particular, only three analyses are available between depths of about 10 and 60 m. The maximum initial $^{234}U/^{238}U$ activity ratios for these analyses (both less than 1.5) are less than the two analyses from about 10 m below the PTn base, as well as many of the values observed in the soil zone. Therefore, ESF initial $^{234}U/^{238}U$ data from this depth interval likely are not representative of the maximum $^{234}U/^{238}U$ ratios of percolating waters and are not included in the subset used to calculate apparent trends. The data represented by filled circles in figure 18 define an exponential curve describing the maximum observed initial $^{234}U/^{238}U$ activity ratio as a function of depth (Maximum Initial $^{234}U/^{238}U = 1.4 * e^{-}$

$^{0.013h}$, where h is the depth below the base of the PTn in meters) defined to depths as much as 150 m below the base of the PTn (fig. 18).

This equation is used to calculate maximum initial $^{234}U/^{238}U$ activity ratios anticipated for hydrogenic minerals in eastern parts of the East-West Cross Drift alignment as a function of distance from the base of the overlying PTn (table 3, fig 17c). Depth of the alignment below the base of the PTn ranges from 79 m at the start of the drift to 253 m beneath the PTn outcrop on the western escarpment of Yucca Mountain. Estimated maximum initial $^{234}U/^{238}U$ activity ratios range from 3.9 at the beginning of the Cross Drift to 9.6 at 1,100 m where the depth below the PTn base is about 150 m. Maximum initial ratios at depths of about 150 m below the base of the PTn range from about 7 to 9 (fig. 18). This range of two units is the basis for using a value of ±1 for the uncertainties of the estimated maximum $^{234}U/^{238}U$ values given in table 3.

Beyond 1,100 m in the Cross Drift alignment, stratigraphic depths exceed those in the ESF. Extrapolation of the curve (fig. 18) to vertical distances greater than 150 m beneath the PTn yields initial $^{234}U/^{238}U$ activity ratios as large as 31 at a point 2,300 m along the alignment, the greatest depth below the PTn base. Values this large have not been observed in southern Nevada ground waters (Ludwig and others, 1993). The largest $^{234}U/^{238}U$ activity ratios yet observed in southern Nevada are from perched and shallow saturated-zone ground water directly beneath Yucca Mountain (generally 8 ± 0.5; Paces and others, 1998). Activity ratios up to 30 have been measured in ground water elsewhere (Osmond and Cowart, 1992); however water with this isotopic composition is rare and confined to reducing environments where uranium solubility is low. Therefore, the high values of initial $^{234}U/^{238}U$ estimated by the equation in figure 18 are considered unreasonable. Either the exponential relation shown in figure 18 is incorrect and requires additional data to define the true relation, or other processes operate to limit the maximum value of initial $^{234}U/^{238}U$ activities in percolating ground water in the Yucca Mountain UZ. Perched and shallow saturated-zone water at Yucca Mountain may provide some information on the limits of maximum $^{234}U/^{238}U$ ratios obtainable in UZ water. However, the amount of mixing of local recharge and flow-through water and exact compositions of the various components is not well understood. Estimates of the maximum $^{234}U/^{238}U$ ratios that may be obtained from minerals in the Cross Drift between 1,100 and 2,300 m are considered beyond the limits of currently available data. Therefore, no values are given for this interval in either table 3 or figure 17c.

Where the PTn is absent in the western parts of the East-West Cross Drift, maximum initial $^{234}U/^{238}U$ activity ratios are expected to be lower. Depths from the surface to the Cross Drift alignment range from 260 to 180 m at distances of 2,350 to 2,800 m. Although the mechanisms producing larger $^{234}U/^{238}U$ activity ratios in percolating solutions are expected to operate along these flow paths, the absence of the PTn should result in greater flux-to-path-length ratios west of the Yucca Crest. An approach similar to the estimates of mineral abundances is adopted for estimating maximum $^{234}U/^{238}U$ ratios in this part of the Cross Drift. Hydrogenic minerals in the Tpc-welded have initial $^{234}U/^{238}U$ activity ratios between 1 and 2 (fig. 18). The lowest values have been affected by artifacts of the subsampling process, but the higher values are consistent with the uranium isotopic compositions in soil water as represented by pedogenic cements at the site (Szabo and others, 1981; Muhs and others, 1990; Paces and others, 1994). Maximum initial $^{234}U/^{238}U$ activity ratios for soil zone carbonates are between 1.9 and 2.0. If these values represent maximum uranium ratios in infiltration, those

of percolation into the deep UZ in the western parts of the Cross Drift where the PTn is absent should be slightly greater. The longer percolation paths between the surface and the Cross Drift should result in greater amounts of excess ^{234}U relative to solutions percolating through the Tpc-welded. Numerical models that describe this isotopic evolution do not exist. Therefore, a value of 3.0 (±1) is selected as a reasonable estimate of the maximum $^{234}U/^{238}U$ activity ratio in areas not overlain by the PTn.

Faulting also may affect maximum initial $^{234}U/^{238}U$ ratios. If faults provide a more direct pathway (shorter path length) or focus greater fluxes, initial $^{234}U/^{238}U$ activity ratios in hydrogenic minerals may be lower than the values estimated in table 3. Neither the Ghost Dance nor Sundance Faults are expected to substantially increase percolation in the areas intersected by the East-West Cross Drift (see section on "Probable Mineral Distribution"). Both the Drill Hole Wash and Solitario Canyon Faults may have a greater effect on UZ flow volume and the resulting $^{234}U/^{238}U$ compositions of percolation and associated hydrogenic minerals. If the effects are substantial, maximum initial $^{234}U/^{238}U$ ratios will be less than the estimate of 4.6 for the Drill Hole Wash fault (150 m in the Cross Drift) and less than 3 near the Solitario Canyon fault (2,500, 2,550, and 2,650 m in the Cross Drift).

SUMMARY AND CONCLUSIONS

Yucca Mountain, in southern Nevada, is the site of a potential geologic repository for high-level radioactive waste. The amount and location of UZ water that may contact waste packages is being investigated. Although percolation flux has not been measured directly, water percolating downward in the past has deposited low-temperature hydrogenic minerals in fracture networks. The past percolation record contained in these minerals can be investigated through physical, chemical and isotopic methods. Mineral data (distributions, ages, and isotopic compositions of calcite and opal in the Exploratory Studies Facility) and interpretations can be used to evaluate conceptual models of UZ flow.

Calcite ($CaCO_3$) and opal ($SiO_2 \cdot nH_2O$) are the two most abundant hydrogenic minerals formed in the subsurface at Yucca Mountain after emplacement and cooling of the host tuffs. Morphologies of hydrogenic-mineral coatings in the UZ are distinct from those below the water table and document interaction between downward-percolating water and upward-migrating vapor that can only occur above the water table. Calcite and opal are present as coatings or partial fillings of fracture cavities and lithophysal voids.

Hydrogenic-mineral abundances measured in the ESF ranged from zero to 0.65 percent. In general, nonwelded tuffs (PTn) with large matrix permeability and few open fractures or cavities have small abundances compared to values in the overlying (Tpc-welded) and underlying (Tpt-welded) welded tuffs. Abundance data for all intervals in welded tuffs have an arithmetic mean of 0.084 percent; however, the frequency distribution is strongly skewed. The data are better represented by a lognormal distribution with a log mean of 0.034 percent. A number of factors may control the distribution of hydrogenic minerals in the subsurface, including topography, infiltration, fracture density, fault and shear frequency, and depth. None of these factors are highly correlated to the measured mineral abundances. Instead, abundances show an apparent decrease with increasing stratigraphic depth and are at least qualitatively associated with fault density. Preferred estimates of mineral abundances grouped by stratigraphic position show an apparent decrease with depth in the welded tuffs of the Tpt-welded with log means of 0.14 percent for the crystal-rich nonlithophysal unit, 0.06 percent for the

crystal-poor upper lithophysal unit, and 0.03 percent for the crystal-poor middle nonlithophysal unit. Uncertainties for percentages in these groups have substantial overlap.

Geochronological data indicate that calcite and opal were deposited at very slow rates. Radiocarbon (46,000 to 16,000 radiocarbon years before present) and ^{230}Th/U (490 to 28 ka) ages for outer mineral surfaces are discordant, but indicate that all dated surfaces are young compared to the 12.7-million-year age of the host tuffs. Textural and isotopic data provide evidence that subsamples represent mixtures of older and younger materials on a micrometer scale. These data include micrometer and smaller laminations in both calcite and opal, large variations in age and initial ^{234}U/^{238}U ratios from multiple subsamples of the same mineral surface, positive correlation between ^{230}Th/U age and subsample thickness, negative correlations between ^{230}Th/U age and calculated initial ^{234}U/^{238}U activity ratio, and the systematic discordance of ages determined by different methods. The range of U-Pb isotope ages for outermost surfaces (1.0 to 0.05 Ma) and interior parts of the mineral coatings (8 to 4 Ma for opal) indicate that average mineral growth rates of 0.5 to 5 mm per million years were maintained in the welded tuffs at the potential repository horizon for at least the last 8 million years. Uniform growth rates during this time period, despite a major climate shift toward increasing aridity, indicate that deep percolation remained relatively constant regardless of variations in meteoric precipitation and infiltration.

Isotopic compositions (δ^{18}O, δ^{13}C, δ^{87}Sr, and initial ^{234}U/^{238}U activity ratios) of calcite and opal deposits in the ESF indicate a soil-zone source for solutes in infiltrating water and vary systematically with depth in the UZ. Hydrogenic calcite δ^{18}O values range from about 19 ± 2 per mil near the surface to about 16 ± 2 per mil at the depth of the potential repository. This pattern is consistent with the theoretical fractionation of oxygen between water and precipitating calcite along an average geothermal gradient of about 34°C/km. In contrast, calcite δ^{13}C values are not correlated with depth but depend on the mineral age. Youngest calcite has δ^{13}C values between about –5 and –9 per mil, whereas intermediate aged calcite has δ^{13}C of –4 to +2 per mil. These ranges are consistent with a soil-gas source of dissolved CO_2; however, soil-gas carbon isotope compositions must have changed during the last 6 m.y. from heavier to lighter δ^{13}C values in order to explain the age-dependent variability in the calcite δ^{13}C values. Strontium isotopes in the ESF calcite also vary with the relative age (δ^{87}Sr values between 3.81 and 4.93 per mil for youngest calcite and 0.42 to 3.95 per mil for older calcite). These variations likely reflect the change in the δ^{87}Sr in the host tuffs over the last 12 m.y. and partial Sr exchange between fluid and vitric tuff in the PTn during percolation. Pore water from core (borehole USW SD-7) has δ^{87}Sr values that vary systematically with depth showing the largest change in δ^{87}Sr in the PTn (average δ^{87}Sr values of 3.67 in the Tpc-welded and 4.65 in the Tpt-welded). Calculated initial ^{234}U/^{238}U activity ratios in calcite and opal also vary from values of 1 to 2 in and above the PTn to values as large as 9.6 in deeper parts of the underlying Tpt-welded. Unlike δ^{87}Sr values, however, the increase in initial ^{234}U/^{238}U ratios occurs below the base of the PTn and is not due to the same process of water-rock interaction. Elevated initial ^{234}U/^{238}U ratios characteristic of minerals in the Tpt-welded require preferential incorporation of ^{234}U into fracture solutions relative to ^{238}U. The large ^{234}U/^{238}U values at Yucca Mountain appear unique relative to recharge areas elsewhere in southern Nevada and likely are caused by low fracture fluxes in the deep UZ.

Hydrogenic-mineral deposits in the ESF contain spatial and temporal information concerning the processes of flow in fractures. Depositional sites in open fractures and cavities and the textures of the mineral deposits imply continuous removal of CO_2 and water vapor resulting in supersaturation of fracture water and deposition of the minerals. Subhorizontal deposition sites are likely the most important areas of water-air exchange indicating that lithophysal zones may play an important role in retarding vertical flow. The lack of hydrogenic minerals in a portion of open cavities exposed in the ESF indicates that these sites have remained isolated from fracture flow. The distribution of hydrogenic-mineral deposits in the shallow units (Tpc-welded and PTn) may be predominantly controlled by the distribution of surface infiltration. At depth (Tpt-welded), however, the availability of throughgoing fractures, depth, and the presence of depositional sites that allow water-air exchange appear to be more important. The decrease of mineral abundances with depth below the base of the PTn is indicative of a general decrease in percolation flux with depth. Uniform long-term rates of deposition determined for mineral coatings below the PTn indicate that the deep UZ may have been buffered from variations in infiltration caused by shifts in Tertiary and Quaternary climate relative to shallower levels. Hydrologic implications based on data from hydrogenic minerals are consistent with concepts of UZ flow proposed by Montazer and Wilson (1984). Data support the conceptualization that the PTn plays an important role in diverting or moderating infiltration flux as well as the presence of a negative flux that advectively removes water-saturated air.

Probable distributions, abundances, and isotopic compositions of hydrogenic minerals elsewhere in Yucca Mountain can be estimated using these UZ paleohydrologic concepts. Mineral-abundance estimates across the potential repository block along the East-West Cross Drift alignment range from 0.0019 to as much as 0.65 percent based on ESF mineral data. The presence of the PTn over most of the East-West Cross Drift is expected to decrease percolation flux, resulting in lower hydrogenic-mineral abundances (typically 0.0019 to 0.060) relative to areas in the western part of the Cross Drift (typically 0.094 to 0.28) where the PTn is absent.

Age estimates for hydrogenic minerals in the Cross Drift are not determined, but, in general, the range of ages in the portions overlain by PTn should be similar to that measured from samples in the Tpt-welded from the ESF. Probable isotopic compositions ($\delta^{18}O$, $\delta^{87}Sr$, and maximum initial $^{234}U/^{238}U$ activity ratio) of hydrogenic minerals are estimated based on depth from the surface and distance between the Cross Drift alignment and the base of the PTn. Estimated calcite $\delta^{18}O$ values vary from 18.0 ± 1 to 16.1 ± 1 per mil as a function of depth below the surface. Calcite $\delta^{87}Sr$ estimates vary with depth below the base of the PTn ranging from about 4.69 ± 0.5 per mil at the eastern end of the alignment to about 4.99 ± 0.5 per mil at a distance of 2,300 m at the western extent of PTn cover. Beyond 2,300 m, $\delta^{87}Sr$ values should be low (about 3.4 per mil) where the PTn is absent, or similar to pedogenic values (about 4.4 per mil) beneath the Solitario Canyon Fault. Estimates of the maximum initial $^{234}U/^{238}U$ ratios are also expected to increase with depth below the PTn from 3.9 at the east end of the alignment to 9.6 at a distance of 1,100 m where the depth below the PTn base exceeds 150 m. Factors controlling the maximimum $^{234}U/^{238}U$ ratios at levels deeper than this are not known, and therefore, estimates are not given between 1,150 and 2,300 m. Beyond 2,300 m, the PTn is generally absent, and maximum initial $^{234}U/^{238}U$ ratios are anticipated to be about 3.0.

Estimates of hydrogenic-mineral distribution and isotopic compositions in this report for the 28-km-long East-West Cross Drift alignment can be compared to observations and analyses of minerals collected from the East-West Cross Drift after completion. The comparison of the observed and estimated data can be used to evaluate the understanding of UZ flow and mineral deposition at Yucca Mountain.

REFERENCES CITED

Bish, D.L., and Chipera, S.J., 1989, Revised mineralogic summary of Yucca Mountain, Nevada: Los Alamos National Lab Report LA-11497-MS, 68 p.

Bodvarsson, G.S., Bandurraga, T.M., and Wu, Y.S., eds., 1997, The site-scale unsaturated zone model at Yucca Mountain, Nevada, for viability assessment: Lawrence Berkeley National Laboratory Report LBNL-40376 UC-814, 749 p.

Broxton, D.E., Bish, D.L., and Warren, R.G., 1987, Distribution and chemistry of diagenic minerals at Yucca Mountain, Nye County, Nevada: Clays and Clay Minerals, v. 35, no. 2, p. 89-110.

Broxton, D.E., Chipera, S.J., Byers, F.M., Jr., and Rautman, C.A., 1993, Geologic evaluation of six nonwelded tuff sites in the vicinity of Yucca Mountain, Nevada, for a surface-based test facility of the Yucca Mountain Project: Los Alamos National Lab Report LA-12542-MS, 83 p.

Buesch, D.C., Spengler, R.W., Moyer, T.C., and Geslin, J.K., 1996, Proposed stratigraphic nomenclature and macroscopic identification of lithostratigraphic units of the Paintbrush Group exposed at Yucca Mountain, Nevada: U.S. Geological Survey Open-File Report 94-469, 47 p.

Byers, F.M., Jr., Carr, W.J., and Orkild, P.P., 1989, Volcanic centers of southwestern Nevada: Evolution of understanding, 1960-1988: Journal of Geophysical Research, v. 94, p. 5908-5924.

Byers, F.M., Jr., Carr, W.J., Orkild, P.P., Quinlivan, W.D., and Sargent, K.A., 1976, Volcanic suites and related cauldrons of Timber Mountain-Oasis Valley caldera complex, southern Nevada: U.S. Geological Survey Professional Paper 919, 70 p.

Carr, W.J., Byers, F.M., Jr., and Orkild, P.P., 1986, Stratigraphic and volcano-tectonic relations of Crater Flat Tuff and some older volcanic units, Nye County, Nevada: U.S. Geological Survey Professional Paper 1323, 23 p.

Christiansen, R.L., Lipman, P.W., Carr, M.J., Byers, F.M., Jr., Orkild, P.P., and Sargent, K.A., 1977, The Timber Mountain – Oasis Valley caldera complex of southern Nevada: Geological Society of America Bulletin, vol. 88, p. 943-959.

Day, W.C., Potter, C.J., Sweetkind, D.S., Dickerson, R.P., and San Juan, C.A., in press, Bedrock geologic map of the central block area, Yucca Mountain, Nevada: U.S. Geological Survey Miscellaneous Investigations Series Map I-2601, scale 1:6,000.

Fabryka-Martin, June, Flint, A.L., Sweetkind, D.S., Wolfsberg, A.V., Levy, S.S., Roemer, G.J.C., Roach, J.L., Wolfsberg, L.E., and Duff, M.C., 1997, Evaluation of flow and transport models of Yucca Mountain, based on chlorine-36 studies for FY97: Los Alamos National Laboratory Milestone Report SP2224M3 to DOE-YMPSCO, Los Alamos National Laboratory Report LA-CST-TIP-97-010, 192 p.

Faunt, C.C., 1997, Effect of faulting on ground-water movement in the Death Valley region, Nevada and California: U.S. Geological Survey Water-Resources Investigations Report 95-4132, 42 p.

Forester, R.M., and Smith, A.J., 1994, Late glacial climate estimates for southern Nevada; The ostracode fossil record, *in* High Level Radioactive Waste Management, Proceedings of the Fifth Annual International Conference, Las Vegas, Nevada, May 22-26, 1994: LaGrange Park, Illinois, American Nuclear Society, vol. 4, p. 2553-2561.

Gascoyne, Mel, 1992, Geochemistry of the actinides and their daughters, *in* Ivanovich, M., and Harmon, R.S., (eds.), Uranium-series disequilibrium: Applications to earth, marine, and environmental sciences (2d ed.): Oxford, U.K., Clarendon Press, p. 34-61.

Hevesi, J.A., Flint, A.L., and Istok, J.D., 1992, Precipitation estimation in mountainous terrain using multivariate geostatistics: II. Isohyetal maps: Journal of Applied Meteorology, v. 31, no. 7, p. 677-678.

Kolm, K.E., and Downey, J.S., 1994, Diverse flow patterns in the aquifers of the Amargosa Desert and vicinity, southern Nevada and California: Bulletin of the Association of Engineering Geologists, v. 31, no. 1, p. 33-47.

Larson, E.E., Patterson, P.E., and Luiszer, F., 1991, Paleoclimate record from ~2.4 to ~0.5 Ma, Tecopa Basin, SE California [abs.]: Geological Society of America Abstracts with Programs, v. 23, no. 5, p. A301.

Levy, S.S., 1991, Mineralogic alteration history and paleohydrology at Yucca Mountain, Nevada, *in* High Level Radioactive Waste Management, Proceedings of the Second Annual International Conference, Las Vegas, Nevada, April 28 – May 3, 1991: LaGrange Park, Illinois, American Nuclear Society, p. 477-485.

Lipman, P.W., Christiansen, R.L., and O'Connor, J.T., 1966, A compositionally zoned ash-flow sheet in southern Nevada: U.S. Geological Survey Professional Paper 524-F, 47 p.

Ludwig, K.R., Simmons, K.R., Szabo, B.J., Winograd, I.J., Landwehr, J.M., Riggs, A.C., and Hoffman, R.J., 1992, Mass-spectrometeric ^{230}Th-^{234}U-^{238}U dating of the Devils Hole calcite vein: Science v. 258, p. 284-287.

Ludwig, K.R., Peterman, Z.E., Simmons, K.R., and Gutentag, E.D., 1993, $^{234}U/^{238}U$ ratios as a ground water flow tracer, SW Nevada-SE California, *in* High Level Radioactive Waste Management, Proceedings of the Fourth Annual International Conference, Las Vegas, Nevada, April 26-30, 1993: LaGrange Park, Illinois, American Nuclear Society, vol. 2, p. 1567-1572.

Marshall, B.D., Futa, Kiyoto, and Peterman, Z.E., in press, Hydrologic inferences from strontium isotopes in pore water from the unsaturated zone at Yucca Mountain, Nevada: Proceedings, Field Testing and Associated Modeling of Potential High-Level Nuclear Waste Geologic Disposal Sites (FTAM) Workshop, Lawrence Berkeley National Laboratory, Nuclear Waste Department, Berkeley, Calif., December 15-16, 1997.

Marshall, B.D. and Mahan, S.A., 1994, Strontium isotope geochemistry of soil and playa deposits near Yucca Mountain, Nevada, *in* High Level Radioactive Waste Management, Proceedings of the Fifth Annual International Conference, Las

Vegas, Nevada, May 22-26, 1994: LaGrange Park, Illinois, American Nuclear Society, vol. 4, p. 2685-2691.

Marshall, B.D., Paces, J.B., Neymark, L.A., Whelan, J.F., and Peterman, Z.E., 1998, Secondary minerals record past percolation flux at Yucca Mountain, Nevada, *in* High Level Radioactive Waste Management, Proceedings of the Ninth Annual International Conference, Las Vegas, Nevada, May 11-14, 1998: LaGrange Park, Illinois, American Nuclear Society, p.

Montazer, Parviz, and Wilson, W.E., 1984, Conceptual hydrological model of flow in the unsaturated zone, Yucca Mountain, Nevada: U.S. Geological Survey Water-Resources Investigation Report 84-4345, 55 p.

Moyer, T.C., Geslin, J.K., and Flint, L.E., 1996, Stratigraphic relations and hydrologic properties of the Paintbrush Tuff nonwelded (PTn) hydrologic unit, Yucca Mountain, Nevada: U.S. Geological Survey Open-File Report 95-397, 151 p.

Muhs, D.R., Whitney, J.W., Shroba, R.R., Taylor, E.M., and Bush, C.A., 1990, Uranium-series dating of secondary carbonates near Yucca Mountain, Nevada: Applications to tectonic, paleomagnetic, and paleohydrologic problems, *in* High Level Radioactive Waste Management, Proceedings of the First Annual International Conference, Las Vegas, Nevada, 1990: LaGrange Park, Illinois, American Nuclear Society, p. 924-929.

Neymark, L.A., Amelin, Yu.V., and Paces, J.B., 1997, Combined U-Pb and ^{230}Th-U dating of Pleistocene opals, Yucca Mountain, Nevada [abs.]: EOS, Transactions of the American Geophysical Union, v. 78, no. 46, p. F788.

Neymark, L.A., Amelin, Yu.V., Paces, J.B., and Peterman, Z.E., 1998, U-Pb age evidence for long-term stability of the unsaturated zone at Yucca Mountain, *in* High Level Radioactive Waste Management, Proceedings of the Ninth Annual International Conference, Las Vegas, Nevada, May 11-14, 1998: LaGrange Park, Illinois, American Nuclear Society, p.

Neymark, L.A. and Paces, J.B., 1996, Mixed isotopic ages as a consequence of very slow rates of deposition in Quaternary subsurface fracture coatings [abs.]: Geological Society of America Abstracts with Programs, v. 28, no. 7, p. A-139.

Noble, D.C, Sargent, K.A., Mehnert, H.H., Ekren, E.B., and Byers, F.M., Jr., 1968, Silent Canyon volcanic center, Nye County, Nevada, *in* Nevada Test Site: Geological Society of America Memoir 110, p. 65-75.

Ortiz, T.S., Williams, R.L., Nimick, F.B., Whittet, B.C., and South, D.L., 1985, A three-dimensional model of reference thermal/mechanical and hydrological stratigraphy at Yucca Mountain, southern Nevada: Sandia Report SAND84-1076, Sandia National Laboratories, Albuquerque, New Mexico, 76 p.

Osmond, J.K., and Cowart, J.B., 1992, Ground water, *in* Ivanovich, M., and Harmon, R.S., (eds.), Uranium-series disequilibrium: Applications to earth, marine, and environmental sciences (2d ed.): Oxford, U.K., Clarendon Press, p. 290-333.

Paces, J.B., Ludwig, K.R., Peterman, Z.E., Neymark, L.A., and Kenneally, J.M., 1998, Anomalous ground-water ^{234}U/^{238}U beneath Yucca Mountain: evidence for local recharge?, *in* High Level Radioactive Waste Management, Proceedings of the Ninth Annual International Conference, Las Vegas, Nevada, May 11-14, 1998: LaGrange Park, Illinois, American Nuclear Society, p.

Paces, J.B., Menges, C.M., Widmann, B.E., Wesling, J.R., Bush, C.A., Futa, Kiyoto, Millard, H.T., Maat, P.B., and Whitney, J.W., 1994, Preliminary U-series disequilibrium and thermoluminescence ages of surficial deposits and paleosols associated with Quaternary faults, eastern Yucca Mountain, *in* High Level Radioactive Waste Management, Proceedings of the Fifth Annual International Conference, Las Vegas, Nevada, May 22-26, 1994: LaGrange Park, Illinois, American Nuclear Society, p. 2391-2401.

Peterman, Z.E., Stuckless, J.S., Marshall, B.D., Mahan, S.A., and Futa, Kiyoto, 1992, Strontium isotope geochemistry of calcite fracture fillings in deep core, Yucca Mountain, Nevada–A progress report, *in* High Level Radioactive Waste Management, Proceedings of the Third Annual International Conference, Las Vegas, Nevada, April 12-16, 1992: LaGrange Park, Illinois, American Nuclear Society: p. 1582-1586.

Rautman, C.A., and Engstrom, D.A., 1996, Geology of the USW SD-12 drill hole, Yucca Mountain, Nevada: Sandia Report SAND96-1368, Sandia National Laboratories, Albuquerque, New Mexico, 131 p.

Robison, J.H., 1984, Ground water level data and preliminary potentiometric-surface maps, Yucca Mountain and vicinity, Nye County, Nevada: U.S. Geological Survey Water-Resources Investigations Report 84-4197, 8 p.

Sass, J.H., and Lachenbruch, A.H., 1982, Preliminary interpretation of thermal data from the Nevada Test Site: U.S. Geological Survey Open-File Report 82-973, 30 p.

Sawyer, D.A., Fleck, R.J., Lanphere, M.A., Warren, R.G., and Broxton, D.E., 1994, Episodic caldera volcanism in the Miocene southwestern Nevada volcanic field: Revised stratigraphic framework, ^{40}Ar/^{39}Ar geochronology, and implications for magmatism and extension: Geological Society of America Bulletin, v. 106, no. 10, p. 1304-1318.

Scott, R.B., and Bonk, Jerry, 1984, Preliminary geologic map of Yucca Mountain, Nye County, Nevada, with geologic sections: U.S. Geological Survey Open-File Report 84-494, 9 p., map scale 1:12,000.

Smith, G.I., 1984, Paleohydrologic regimes in the southwestern Great Basin, 0-3.2 my ago, compared with other long records of "global" climate: Quaternary Research, v. 22, p. 1-17.

Spaulding, W.G., 1985, Vegetation and climates of the last 45,000 years in the vicinity of the Nevada Test Site, south-central Nevada: U.S. Geological Survey Professional Paper 1329, 83 p.

Szabo, B.J., and Kyser, T.K., 1990, Ages and stable-isotope compositions of secondary calcite and opal in drill cores from Tertiary volcanic rocks of the Yucca Mountain area, Nevada: Geological Society of America Bulletin, v. 102, no. 12, p. 1714-1719.

Szabo, B.J., Carr, W.J., and Gottschall, W.C., 1981, Uranium-thorium dating of Quaternary carbonate accumulations in the Nevada Test Site region, southern Nevada: U.S. Geological Survey Open-File Report 81-119, 35 p.

Thompson, R.S., 1991, Pliocene environments and climates in the western United States: Quaternary Science Reviews, v. 10, no. 1, p. 115-132.

Tokunaga, T.K., and Wan, J., 1997, Water film flow along fracture surfaces of porous rock: Water Resources Research, v. 33, no. 6, p. 1287-1295.

TRW Environmental Safety Systems, Inc., 1998, ECRB predictive geotechnical report – Volume 1: Geotechnical baseline report:

Las Vegas, Nev., TRW Environmental Safety Systems Report BABEA0000-01717-5705-00002 Revision 0, 106 p.

Tucci, Patrick, and Burkhardt, D.J., 1995, Potentiometric-surface map, 1993, Yucca Mountain and vicinity, Nevada: U.S. Geological Survey Water-Resources Investigations Report 95-4149, 15 p.

Vaniman, D.T., 1993, Calcite deposits in fractures at Yucca Mountain, Nevada, *in* High Level Radioactive Waste Management, Proceedings of the Fourth Annual International Conference, Las Vegas, Nevada, April 26-30, 1993: LaGrange Park, Illinois, American Nuclear Society, vol. 2, p. 1935-1939.

Vaniman, D.T., 1994, Calcite deposits in drill cores USW G-2 and USW GU-3/G-3 at Yucca Mountain, Nevada; Preliminary Report: Los Alamos National Laboratory Report LA-12720-MS, 28 p.

Whelan, J.F., and Moscati, R.F., 1998, 9 m.y. record of southern Nevada climate from Yucca Mountain secondary minerals, *in* High Level Radioactive Waste Management, Proceedings of the Ninth Annual International Conference, Las Vegas, Nevada, May 11-14, 1998: LaGrange Park, Illinois, American Nuclear Society, p.

Whelan, J.F., and Stuckless, J.S., 1992, Paleohydrologic implications of the stable isotopic composition of secondary calcite within the Tertiary volcanic rocks of Yucca Mountain, Nevada, *in* High Level Radioactive Waste Management, Proceedings of the Third Annual International Conference, Las Vegas, Nevada, April 12-16, 1992: LaGrange Park, Illinois, American Nuclear Society, p. 1572-1581.

Whelan, J.F., Vaniman, D.T., Stuckless, J.S., and Moscati, R.J., 1994, Paleoclimatic and paleohydrologic records from secondary calcite: Yucca Mountain, Nevada, *in* High Level Radioactive Waste Management, Proceedings of the Fifth Annual International Conference, Las Vegas, Nevada, May 22-26, 1994: LaGrange Park, Illinois, American Nuclear Society, vol. 4, p. 2738-2745.

Winograd, I.J., Coplen, T.B., Landwehr, J.M., Riggs, A.C., Ludwig, K.R., Szabo, B.J., Kolesar, P.T., and Revesz, K.M., 1992, Continuous 500,000-year climate record from vein calcite in Devils Hole, Nevada: Science, v. 258, p. 255-260.

Winograd, I.J., Szabo, B.J., Coplen, T.B., Riggs, A.C., and Kolesar, P.T., 1985, Two-million-year record of deuterium depletion in Great Basin ground waters: Science, v. 227, p. 519-522.

Zielinski, R.A., 1980, Uranium in secondary silica: a possible exploration guide: Economic Geology, vol. 75, p. 592-602.

Table 1. Calcite and opal abundances in the Exploratory Studies Facility (ESF)

[Individual survey intervals are 60-centimeter-wide bands centered on a 30-meter-long tape stretched along the right rib of the ESF at a height of about 1.2 to 1.7 meters above the concrete invert. Thickness and width of individual calcite and opal deposits in this band are used to calculate areas of hydrogenic minerals, which are summed and divided by the total area of uncovered rock wall within the band to obtain abundances in percent. ESF stations are linear distances in meters starting from the north portal. Stratigraphic units are from Buesch and others (1996). No., number; lith, lithophysal; nonlith, nonlithophysal; Tpc-w, Tiva Canyon welded; PTn, Paintbrush Tuff nonwelded; Tpt-w, Topopah Spring welded; (---), tuffs not belonging to Paintbrush Group; n.a., not applicable; dup, duplicate]

Survey identifier	ESF station, start	No. of deposits	Calcite and opal abundance		Hydro-geologic unit	Stratigraphic unit		
			All forms[1]	Lithophysae only		Abbrev-iation	Formation	Zone
19971202-01a	100	18	0.20	0.002	Tpc-w	Tpcpmn	Tiva Canyon Tuff	Middle nonlith
19971202-02a	200	3	0.089	0.000	n.a.	Pre-Rainier BT	---	---
19971202-03a	300	1	0.008	0.000	n.a.	Tuff 'X'	---	---
19971202-04a	400	3	0.068	0.000	Tpc-w	Tpcrn	Tiva Canyon Tuff	Nonlith
19971202-05a	500	8	0.083	0.006	Tpc-w	Tpcpul	Tiva Canyon Tuff	Upper lith
19971202-06a	600	13	0.078	0.000	Tpc-w	Tpcpll-Tpcpln	Tiva Canyon Tuff	Lower lith-lower nonlith
19971202-07a	700	8	0.042	0.000	Tpc-w	Tpcpln	Tiva Canyon Tuff	Lower nonlith
19971202-08a	800	0	0.000	0.000	PTn	Tpcpv	Tiva Canyon Tuff	Vitric
19971202-09a	900	0	0.000	0.000	PTn	Tpp	Pah Canyon Tuff	n.a.
19971202-10a	1000	1	0.007	0.000	PTn	Tpp	Pah Canyon Tuff	n.a.
19960625-11a	1100	3	0.013	0.000	PTn	Tptrv	Topopah Spring Tuff	Nonlith
19960625-12a	1200	4	0.061	0.000	Tpt-w	Tptrn	Topopah Spring Tuff	Nonlith
19960625-13a	1300	10	0.37	0.000	Tpt-w	Tptrn	Topopah Spring Tuff	Nonlith
19960625-14a	1400	2	0.10	0.000	Tpt-w	Tptrn	Topopah Spring Tuff	Nonlith
19960625-15a	1500	8	0.10	0.009	Tpt-w	Tptrn	Topopah Spring Tuff	Nonlith
19960625-16a	1600	4	0.25	0.001	Tpt-w	Tptrn	Topopah Spring Tuff	Nonlith
19960625-17a	1700	0	0.000	0.000	Tpt-w	Tptrn-Tptrl	Topopah Spring Tuff	Nonlith – lith transition
19960625-18a	1800	0	0.000	0.000	Tpt-w	Tptpul	Topopah Spring Tuff	Upper lith
19960625-19a	1900	1	0.013	0.000	Tpt-w	Tptpul	Topopah Spring Tuff	Upper lith
19960625-20a	2000	2	0.016	0.016	Tpt-w	Tptpul	Topopah Spring Tuff	Upper lith
19960625-21a	2100	0	0.000	0.000	Tpt-w	Tptpul	Topopah Spring Tuff	Upper lith

Table 1. Calcite and opal abundances in the Exploratory Studies Facility (ESF) – Continued

Survey identifier	ESF station, start	No. of deposits	Calcite and opal abundance		Hydro-geologic unit	Stratigraphic unit		
			All forms[1]	Lithophysae only		Abbrev-iation	Formation	Zone
19960712-22a	2200	36	0.65	0.25	Tpt-w	Tptpul	Topopah Spring Tuff	Upper lith
19960625-22a (dup)[2]	2200	29	0.48	0.31	Tpt-w	Tptpul	Topopah Spring Tuff	Upper lith
19960712-23a	2300	1	0.003	0.003	Tpt-w	Tptpul	Topopah Spring Tuff	Upper lith
19960712-24a	2400	8	0.057	0.057	Tpt-w	Tptpul	Topopah Spring Tuff	Upper lith
19960712-25a	2500	6	0.026	0.026	Tpt-w	Tptpul	Topopah Spring Tuff	Upper lith
19960712-26a	2600	17	0.14	0.14	Tpt-w	Tptpul	Topopah Spring Tuff	Upper lith
19960712-27a	2700	14	0.30	0.30	Tpt-w	Tptpul-Tptpmn	Topopah Spring Tuff	Upper lith-middle nonlith
19960712-27b	2750	2	0.009	0.009	Tpt-w	Tptpmn	Topopah Spring Tuff	Middle nonlith
19960712-29a	2900	12	0.25	0.10	Tpt-w	Tptpmn	Topopah Spring Tuff	Middle nonlith
19960712-30a	3000	4	0.43	0.43	Tpt-w	Tptpmn	Topopah Spring Tuff	Middle nonlith
19971201-31a	3120	13	0.036	0.036	Tpt-w	Tptpmn	Topopah Spring Tuff	Middle nonlith
19971201-32a	3200	2	0.004	0.004	Tpt-w	Tptpmn	Topopah Spring Tuff	Middle nonlith
19971201-33a	3300	7	0.076	0.060	Tpt-w	Tptpmn	Topopah Spring Tuff	Middle nonlith
19971202-34a	3400	8	0.087	0.000	Tpt-w	Tptpmn	Topopah Spring Tuff	Middle nonlith
19961218-35a	3500	12	0.068	0.004	Tpt-w	Tptpmn	Topopah Spring Tuff	Middle nonlith
19961218-36a	3600	2	0.001	0.000	Tpt-w	Tptpmn	Topopah Spring Tuff	Middle nonlith
19971202-36b	3670	2	0.018	0.000	Tpt-w	Tptpmn	Topopah Spring Tuff	Middle nonlith
19961218-38a	3800	4	0.011	0.011	Tpt-w	Tptpmn	Topopah Spring Tuff	Middle nonlith
19961218-39a	3900	8	0.066	0.010	Tpt-w	Tptpmn	Topopah Spring Tuff	Middle nonlith
19961218-40a	4000	1	0.003	0.000	Tpt-w	Tptpmn	Topopah Spring Tuff	Middle nonlith
19961218-41a	4100	5	0.039	0.000	Tpt-w	Tptpmn	Topopah Spring Tuff	Middle nonlith
19961218-42a	4200	8	0.031	0.000	Tpt-w	Tptpmn	Topopah Spring Tuff	Middle nonlith
19961218-43a	4300	4	0.016	0.000	Tpt-w	Tptpmn	Topopah Spring Tuff	Middle nonlith
19961218-44a	4400	1	0.005	0.000	Tpt-w	Tptpmn	Topopah Spring Tuff	Middle nonlith
19961218-45a	4500	3	0.10	0.000	Tpt-w	Tptpmn	Topopah Spring Tuff	Middle nonlith
19961218-46a	4600	5	0.026	0.000	Tpt-w	Tptpmn	Topopah Spring Tuff	Middle nonlith

Table 1. Calcite and opal abundances in the Exploratory Studies Facility (ESF) – Continued

Survey identifier	ESF station, start	No. of deposits	Calcite and opal abundance		Hydro-geologic unit	Stratigraphic unit		
			All forms[1]	Lithophysae only		Abbrev-iation	Formation	Zone
19961218-47a	4700	4	0.011	0.000	Tpt-w	Tptpmn	Topopah Spring Tuff	Middle nonlith
19961218-48a	4800	6	0.029	0.000	Tpt-w	Tptpmn	Topopah Spring Tuff	Middle nonlith
19961218-49a	4900	11	0.078	0.000	Tpt-w	Tptpmn	Topopah Spring Tuff	Middle nonlith
19961008-49a (dup)[2]	4900	4	0.029	0.000	Tpt-w	Tptpmn	Topopah Spring Tuff	Middle nonlith
19961008-50a	5000	2	0.052	0.000	Tpt-w	Tptpmn	Topopah Spring Tuff	Middle nonlith
19961008-51a	5100	9	0.29	0.000	Tpt-w	Tptpmn	Topopah Spring Tuff	Middle nonlith
19961008-52a	5200	2	0.050	0.000	Tpt-w	Tptpmn	Topopah Spring Tuff	Middle nonlith
19961008-53a	5300	6	0.041	0.000	Tpt-w	Tptpmn	Topopah Spring Tuff	Middle nonlith
19961008-54a	5400	5	0.058	0.000	Tpt-w	Tptpmn	Topopah Spring Tuff	Middle nonlith
19961008-55a	5500	7	0.057	0.000	Tpt-w	Tptpmn	Topopah Spring Tuff	Middle nonlith
19961008-56a	5600	14	0.074	0.000	Tpt-w	Tptpmn	Topopah Spring Tuff	Middle nonlith
19961008-57a	5700	1	0.002	0.000	Tpt-w	Tptpmn	Topopah Spring Tuff	Middle nonlith
19961008-58a	5800	0	0.000	0.000	Tpt-w	Tptpll	Topopah Spring Tuff	Lower lith
19961008-59a	5900	0	0.000	0.000	Tpt-w	Tptpmn	Topopah Spring Tuff	Middle nonlith
19961008-60a	6000	6	0.11	0.000	Tpt-w	Tptpmn	Topopah Spring Tuff	Middle nonlith
19961008-61a	6100	3	0.039	0.000	Tpt-w	Tptpmn	Topopah Spring Tuff	Middle nonlith
19961008-62a	6200	4	0.071	0.000	Tpt-w	Tptpmn	Topopah Spring Tuff	Middle nonlith
19961217-63a	6300	17	0.12	0.012	Tpt-w	Tptpmn-Tptpul	Topopah Spring Tuff	Middle nonlith - upper lith
19961008-63a (dup)[2]	6300	23	0.22	0.032	Tpt-w	Tptpmn-Tptpul	Topopah Spring Tuff	Middle nonlith - upper lith
19961217-64a	6400	2	0.020	0.020	Tpt-w	Tptpul	Topopah Spring Tuff	Upper lith
19961217-65a	6500	3	0.012	0.012	Tpt-w	Tptrl-Tptrn	Topopah Spring Tuff	Lith – nonlith
19961217-66a	6600	1	0.033	0.000	Tpt-w	Tptrn	Topopah Spring Tuff	Nonlith
19961217-67a	6700	0	0.000	0.000	PTn	Tpcpv	Tiva Canyon Tuff	Vitric
19961217-68a	6800	1	0.060	0.060	Tpt-w	Tptpul	Topopah Spring Tuff	Upper lith
19961217-69a	6900	2	0.029	0.000	Tpt-w	Tptrn	Topopah Spring Tuff	Nonlith
19970715-71a	7100	4	0.21	0.000	Tpt-w	Tptpmn	Topopah Spring Tuff	Middle nonlith

Table 1. Calcite and opal abundances in the Exploratory Studies Facility (ESF) – Continued

Survey identifier	ESF station, start	No. of deposits	Calcite and opal abundance		Hydro-geologic unit	Stratigraphic unit		
			All forms[1]	Lithophysae only		Abbrev-iation	Formation	Zone
19970715-71b	7170	22	0.062	0.052	Tpt-w	Tptpul	Topopah Spring Tuff	Upper lith
19970715-72a	7200	15	0.030	0.026	Tpt-w	Tptpul	Topopah Spring Tuff	Upper lith
19970715-73a	7300	6	0.038	0.026	Tpt-w	Tptrl	Topopah Spring Tuff	Lith
19970715-74a	7400	14	0.050	0.000	Tpt-w	Tptrn	Topopah Spring Tuff	Nonlith
19970715-75a	7500	12	0.045	0.000	PTn-Tpc-w	Tpcpv-Tpcpln	Tiva Canyon Tuff	Vitric - lower nonlith
19970715-76a	7600	10	0.17	0.000	Tpc-w	Tpcpln-Tpcpmn	Tiva Canyon Tuff	Lower nonlith - middle nonlith
19970715-77a	7700	24	0.21	0.000	Tpc-w	Tpcpmn	Tiva Canyon Tuff	Middle nonlith
19970715-78a	7800	11	0.11	0.096	Tpc-w	Tpcpmn	Tiva Canyon Tuff	Middle nonlith

[1] All forms of hydrogenic mineral deposits include coatings in fracture cavities, breccia zones, lithophysae, and vapor phase partings (extremely flattened lithophysae).
[2] Duplicate surveys are not used to calculate means. The most recent of the two surveys is used as the best estimate.

Table 2. Summary of calcite and opal abundances in the Exploratory Studies Facility (ESF) grouped by stratigraphic unit and location

[All means, medians, uncertainties and standard deviations are given in percent. Stratigraphic units are from Buesch and others (1996). σ, standard deviation; n.a., not applicable; ESF locations are given as NR, north ramp, SR, south ramp, and MD, main drift]

Stratigraphic unit		ESF location	Number of intervals	Statistical measures of calcite and opal abundances: Arithmetic[1] Mean	Arithmetic[1] σ	Logarithmic[2] Mean	Logarithmic[2] (Uncertainty)	Logarithmic[2] σ	Median	Mean number of deposits[3]
	Pre-Rainier BT	NR	1	0.089	n.a.	0.089	(+0.18/-0.06)	n.a.	0.089	3
	Tuff 'X'	NR	1	0.008	n.a.	0.008	(+0.02/-0.005)	n.a.	0.008	1
Tiva Canyon Tuff - welded (Tpc-w)										
Tpcrn	Crystal-rich nonlithophysal	NR	1	0.068	n.a.	0.068	(+0.14/-0.05)	n.a.	0.068	3
Tpcpul	Upper lithophysal	NR	1	0.083	n.a.	0.083	(+0.17/-0.06)	n.a.	0.083	8
Tpcpmn	Middle nonlithophysal	NR+SR	4	0.17	0.07	0.16	(+0.10/-0.06)	+0.06/-0.04	0.18	15
Tpcpln	Lower nonlithophysal	NR+SR	3	0.055	0.02	0.053	(+0.07/-0.03)	+0.02/-0.015	0.045	11
	Average of all Tpc-w subunits	NR+SR	9	0.11	0.06	0.094	(+0.05/-0.03)	+0.08/-0.04	0.083	11.9
Paintbrush Tuff nonwelded (PTn)										
Tpcpv	Crystal-poor vitric	NR+SR	2	0.000	0.0	0.000	0	n.a.	0.000	0
Tpbt3-Tpp	Pah Canyon Tuff	NR	1	0.000	n.a.	0.000	0	n.a.	0.000	0
Tpp-Tpbt2	Pah Canyon Tuff	NR	1	0.007	n.a.	0.007	(+0.014/-0.005)	n.a.	0.007	1
Tptrv	Crystal-rich vitrophyre	NR	1	0.013	n.a.	0.013	(+0.03/-0.009)	n.a.	0.013	3
Topopah Spring Tuff - welded (Tpt-w)										
Tptrn	Crystal-rich nonlithophysal	NR	5	0.18	0.13	0.14	(+0.2/-0.08)	+0.16/-0.07	0.10	5.6
Tptrn	Crystal-rich nonlithophysal	SR	4	0.031	0.016	0.028	(+0.04/-0.017)	+0.02/-0.012	0.031	5
Tptpul	Upper lithophysal	NR	11	0.11	0.20	0.014	(+0.07/-0.011)	+0.17/-0.013	0.016	7.7
Tptpul	Upper lithophysal	NR[4]	4	0.13	0.12	0.090	(+0.4/-0.07)	+0.17/-0.06	0.10	11.2
Tptpul	Upper lithophysal	SR	6	0.055	0.036	0.047	(+0.04/-0.02)	+0.04/-0.02	0.049	10.5
Tptpul	Upper lithophysal	NR[4]+SR	10	0.086	0.086	0.060	(+0.05/-0.03)	+0.08/-0.03	0.059	10.8

Table 2. Summary of calcite and opal abundances in the Exploratory Studies Facility (ESF) grouped by stratigraphic unit and location – Continued

Lithostratigraphic units		ESF location	Number of intervals	Statistical measures of calcite and opal abundances						Mean number of deposits[3]
				Arithmetic[1]		Logarithmic[2]			Median	
				Mean	σ	Mean	(uncertainty)	σ		
Tptpmn	Middle nonlithophysal	MD	30	0.067	0.09	0.030	(+0.02/-0.010)	+0.10/-0.02	0.040	5.7
Tptpmn	Middle nonlithophysal	SR	5	0.086	0.08	0.032	(+0.6/-0.03)	+0.3/-0.03	0.07	3.4
Tptpll	Lower lithophysal	MD	1	0.000	n.a.	0.000	n.a.	n.a.	0.000	0

[1] Arithmetic mean and standard deviation (σ) are based on the total number of 30-meter survey intervals given in preceding column. The values for individual surveys are given where only a single survey is available for a given stratigraphic unit.

[2] Log mean is the arithmetic mean of the log of the 30-meter survey data. Uncertainties, in parentheses, are at the 95-percent confidence level and represent mean errors calculated using the standard deviation of the mean and a Student-t multiplier that is dependent on the number of values used. Uncertainties for groups with only a single interval have a +error = 3m-m and –error = m-0.33m, where m is the log mean value of the individual survey, and the values 3 and 0.33 are derived from the maximum allowable measurement errors based on duplicate surveys. Standard deviations (σ) are calculated from the log of the percentage values.

[3] Mean number of deposits is the average number of calcite and opal deposits per 30-meter interval over the stated number of intervals.

[4] Mean calculations exclude surveys underlying Drill Hole Wash because of anomalous structural features and topography that are not present over most of the potential repository block.

Table 3. Estimates of the abundance of and selected isotopic compositions for calcite and opal in the East-West Cross Drift

[Methods, assumptions and limitations for parameter estimates are given in the text. Uncertainties are given at the two standard deviation level. Stratigraphic units, Depth from land surface, and Depth from PTn base are measured from cross sections in TRW Environmental Safety Systems, Inc. (1998). Numerical estimates are carried to one digit beyond the last significant figure for plotting purposes. Values are queried where uncertain. Distance in Cross Drift and all depths are given in meters. Stratigraphic nomenclature is from Buesch and others (1996). Values for delta oxygen-18 ($\delta^{18}O$) and delta strontium-87 ($\delta^{87}Sr$) are given as per mil deviations from sea water standards. Exploratory Studies Facility (ESF) station nomenclature indicates distance, in hundreds of meters, from the north portal. DHWF, Drill Hole Wash Fault; GDF, Ghost Dance Fault; SDF, Sundance Fault; SCF, Solitario Canyon Fault; n.p., not present; <, less than; --, no basis for estimation]

Cross Drift distance	Strati-graphic unit	Depth from land surface	Depth from PTn base	Estimated hydrogenic-mineral abundance[1]		Isotopic compositions of outermost mineral layers		
				Percent	Remarks	$\delta^{18}O$	$\delta^{87}Sr$	Maximum initial $^{234}U/^{238}U_{activity}$
0	Tptpul	180	79	0.016 (+0.032/-0.011)	ESF station 20 value	18.0 (±1)	4.69 (±0.5)	3.9 (±1)
50	Tptpul	180	83	0.016 (+0.032/-0.011)	ESF station 20 value	18.0 (±1)	4.69 (±0.5)	4.1 (±1)
100	Tptpul	180	86	0.0019 (+0.076/-0.0018)	Log mean ESF stations 17-21	18.0 (±1)	4.70 (±0.5)	4.3 (±1)
150	Tptpul	180	91	0.65 (+1.3/-0.43)	DHWF: ESF station 22 value	18.0 (±1)	4.71 (±0.5)	4.6 (±1)
200	Tptpul	190	95	0.0019 (+0.076/-0.0018)	Log mean ESF stations 17-21	17.9 (±1)	4.71 (±0.5)	4.8 (±1)
250	Tptpul	210	100	0.060 (+0.27/-0.049)	Log mean Tptpul value	17.7 (±1)	4.72 (±0.5)	5.1 (±1)
300	Tptpul	230	107	0.060 (+0.27/-0.049)	Log mean Tptpul value	17.5 (±1)	4.73 (±0.5)	5.6 (±1)
350	Tptpul	215	112	0.060 (+0.27/-0.049)	Log mean Tptpul value	17.7 (±1)	4.74 (±0.5)	5.9 (±1)
400	Tptpul	200	115	0.060 (+0.27/-0.049)	Log mean Tptpul value	17.8 (±1)	4.75 (±0.5)	6.2 (±1)
450	Tptpul	185	120	0.060 (+0.27/-0.049)	GDF (minimal effect): log mean Tptpul value	18.0 (±1)	4.76 (±0.5)	6.6 (±1)
500	Tptpul	190	125	0.060 (+0.27/-0.049)	GDF (minimal effect): log mean Tptpul value	17.9 (±1)	4.77 (±0.5)	7.0 (±1)
550	Tptpul	210	126	0.060 (+0.27/-0.049)	Log mean Tptpul value	17.7 (±1)	4.77 (±0.5)	7.1 (±1)
600	Tptpul	240	128	0.060 (+0.27/-0.049)	Log mean Tptpul value	17.4 (±1)	4.77 (±0.5)	7.2 (±1)
650	Tptpul	255	129	0.060 (+0.27/-0.049)	Log mean Tptpul value	17.2 (±1)	4.77 (±0.5)	7.3 (±1)
700	Tptpul	270	131	0.43 (+0.86/-0.29)	ESF station 30 value	17.1 (±1)	4.78 (±0.5)	7.5 (±1)
750	Tptpul	245	132	0.036 (+0.072/-0.024)	ESF station 31 value	17.4 (±1)	4.78 (±0.5)	7.6 (±1)
800	Tptpul	240	133	0.004 (+0.008/-0.0027)	ESF station 32 value	17.4 (±1)	4.78 (±0.5)	7.7 (±1)
850	Tptpul	260	136	0.060 (+0.27/-0.049)	Log mean Tptpul value	17.2 (±1)	4.78 (±0.5)	8.0 (±1)

Table 3: Estimates of the abundance of and selected isotopic compositions for calcite and opal in the East-West Cross Drift – Continued

Cross Drift distance	Strati-graphic unit	Depth from land surface	Depth from PTn base	Estimated hydrogenic-mineral abundance[1]		Isotopic compositions of outermost mineral layers		
				Percent	Remarks	$\delta^{18}O$	$\delta^{87}Sr$	Maximum initial $^{234}U/^{238}U_{activity}$
900	Tptpul	260	139	0.060 (+0.27/-0.049)	Log mean Tptpul value	17.2 (±1)	4.79 (±0.5)	8.3 (±1)
950	Tptpul	245	140	0.060 (+0.27/-0.049)	Log mean Tptpul value	17.4 (±1)	4.79 (±0.5)	8.4 (±1)
1000	Tptpul	240	142	0.060 (+0.27/-0.049)	Log mean Tptpul value	17.4 (±1)	4.79 (±0.5)	8.6 (±1)
1050	Tptpul	255	147	0.060 (+0.27/-0.049)	SDF (minimal effect): log mean Tptpul value	17.2 (±1)	4.80 (±0.5)	9.2 (±1)
1100	Tptpmn	280	151	0.030 (+0.52/-0.028)	SDF (minimal effect): log mean Tptpmn value	17.0 (±1)	4.81 (±0.5)	9.6 (±1)
1150	Tptpmn	290	154	0.030 (+0.52/-0.028)	Log mean Tptpmn value	16.9 (±1)	4.81 (±0.5)	--
1200	Tptpmn	280	158	0.030 (+0.52/-0.028)	Log mean Tptpmn value	17.0 (±1)	4.82 (±0.5)	--
1250	Tptpmn	260	161	0.030 (+0.52/-0.028)	Log mean Tptpmn value	17.2 (±1)	4.83 (±0.5)	--
1300	Tptpmn	285	165	0.030 (+0.52/-0.028)	Log mean Tptpmn value	16.9 (±1)	4.83 (±0.5)	--
1350	Tptpmn	305	167	0.030 (+0.52/-0.028)	Log mean Tptpmn value	16.7 (±1)	4.84 (±0.5)	--
1400	Tptpmn	300	171	0.030 (+0.52/-0.028)	Log mean Tptpmn value	16.8 (±1)	4.84 (±0.5)	--
1450	Tptpmn	300	174	0.030 (+0.52/-0.028)	Log mean Tptpmn value	16.8 (±1)	4.85 (±0.5)	--
1500	Tptpmn	290	178	0.030 (+0.52/-0.028)	Log mean Tptpmn value	16.9 (±1)	4.86 (±0.5)	--
1550	Tptpmn	280	182	0.030 (+0.52/-0.028)	Log mean Tptpmn value	17.0 (±1)	4.86 (±0.5)	--
1600	Tptpmn	285	185	0.030 (+0.52/-0.028)	Log mean Tptpmn value	16.9 (±1)	4.87 (±0.5)	--
1650	Tptpmn-Tptpll	310	191	0.030 (+0.52/-0.028)	Log mean Tptpmn value	16.7 (±1)	4.88 (±0.5)	--
1700	Tptpll	330	196	0.010 (+0.17/-0.0095)	0.33*log mean Tptpmn value	16.5 (±1)	4.89 (±0.5)	--
1750	Tptpll	335	202	0.010 (+0.17/-0.0095)	0.33*log mean Tptpmn value	16.4 (±1)	4.90 (±0.5)	--
1800	Tptpll	345	206	0.010 (+0.17/-0.0095)	0.33*log mean Tptpmn value	16.3 (±1)	4.90 (±0.5)	--
1850	Tptpll	355	210	0.010 (+0.17/-0.0095)	0.33*log mean Tptpmn value	16.2 (±1)	4.91 (±0.5)	--
1900	Tptpll	360	215	0.010 (+0.17/-0.0095)	0.33*log mean Tptpmn value	16.2 (±1)	4.92 (±0.5)	--
1950	Tptpll	365	218	0.010 (+0.17/-0.0095)	0.33*log mean Tptpmn value	16.1 (±1)	4.92 (±0.5)	--

Table 3: Estimates of the abundance of and selected isotopic compositions for calcite and opal in the East-West Cross Drift – Continued

Cross Drift distance	Strati-graphic unit	Depth from land surface	Depth from PTn base	Estimated hydrogenic-mineral abundance[1]		Isotopic compositions of outermost mineral layers		
				Percent	Remarks	$\delta^{18}O$	$\delta^{87}Sr$	Maximum initial $^{234}U/^{238}U_{activity}$
2000	Tptpll	370	223	0.010 (+0.17/-0.0095)	0.33*log mean Tptpmn value	16.1 (±1)	4.93 (±0.5)	--
2050	Tptpll	370	228	0.010 (+0.17/-0.0095)	0.33*log mean Tptpmn value	16.1 (±1)	4.94 (±0.5)	--
2100	Tptpll	350	233	0.010 (+0.17/-0.0095)	0.33*log mean Tptpmn value	16.3 (±1)	4.95 (±0.5)	--
2150	Tptpll	325	239	0.010 (+0.17/-0.0095)	0.33*log mean Tptpmn value	16.5 (±1)	4.96 (±0.5)	--
2200	Tptpll	300	244	0.010 (+0.17/-0.0095)	0.33*log mean Tptpmn value	16.8 (±1)	4.97 (±0.5)	--
2250	Tptpll	285	250	0.010 (+0.17/-0.0095)	0.33*log mean Tptpmn value	16.9 (±1)	4.98 (±0.5)	--
2300	Tptpll	270	253	0.010 (+0.17/-0.0095)	0.33*log mean Tptpmn value	17.1 (±1)	4.99 (±0.5)	--
2350	Tptpln	260	n.p.	0.094 (+0.22/-0.065)	No PTn: log mean TCw value	17.2 (±1)	3.4 (±1.1)	3.0 (±1)
2400	Tptpln	245	n.p.	0.094 (+0.22/-0.065)	No PTn: log mean TCw value	17.4 (±1)	3.4 (±1.1)	3.0 (±1)
2450	Tptpln	225	n.p.	0.094 (+0.22/-0.065)	No PTn: log mean TCw value	17.6 (±1)	3.4 (±1.1)	3.0 (±1)
2500	Tptpln	210	n.p.	0.28 (+0.66/-0.20)	SCF: log mean TCw value*3	17.7 (±1)	3.4 (±1.1)	3.0 (±1)
2550	Tptpll	200	80	0.28 (+0.66/-0.20)	SCF: log mean TCw value*3	17.8 (±1)	3.4 (±1.1)	3.0 (±1)
2600	Tptpul	190	71	0.060 (+0.27/-0.049)	PTn present: log mean Tptpul value	17.9 (±1)	4.4 (±0.8)	3.0 (±1)
2650	Tptpmn-Tptpll	185	60?	0.28 (+0.66/-0.20)	SCF: log mean TCw value*3	18.0 (±1)	4.4 (±0.8)	3.0 (±1)
2700	Tptpmn	180	n.p.	0.094 (+0.22/-0.065)	No PTn: log mean TCw value	18.0 (±1)	4.4 (±0.8)	3.0 (±1)
2750	PTn	180	-14	<0.005	PTn value	18.0 (±1)	4.4 (±0.8)	3.0 (±1)
2800	PTn-Tptrn	180	0	<0.005	PTn value	18.0 (±1)	4.4 (±0.8)	3.0 (±1)

[1] Mineral abundances are estimated from the selected log-mean values given in table 2, from abundances in nearby ESF mineral survey intervals, or from hypothetical values described in the remarks column and in the text. Uncertainties are two log standard deviations for values estimated from stratigraphic units with multiple intervals, and +200%/-0.667% of the values estimated for units with only one measured interval.

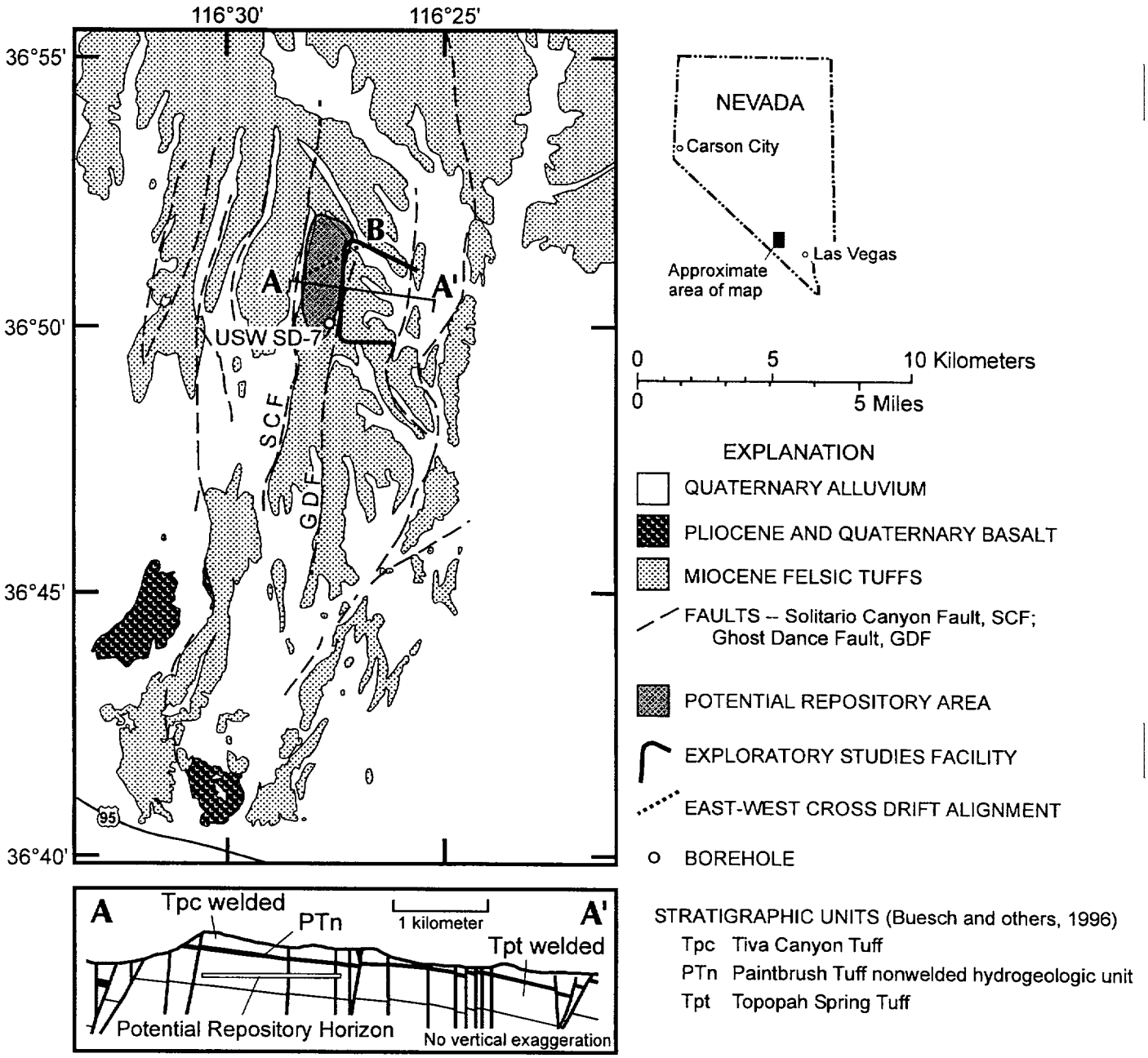

Figure 1. Geologic map and cross section of Yucca Mountain, Nevada.

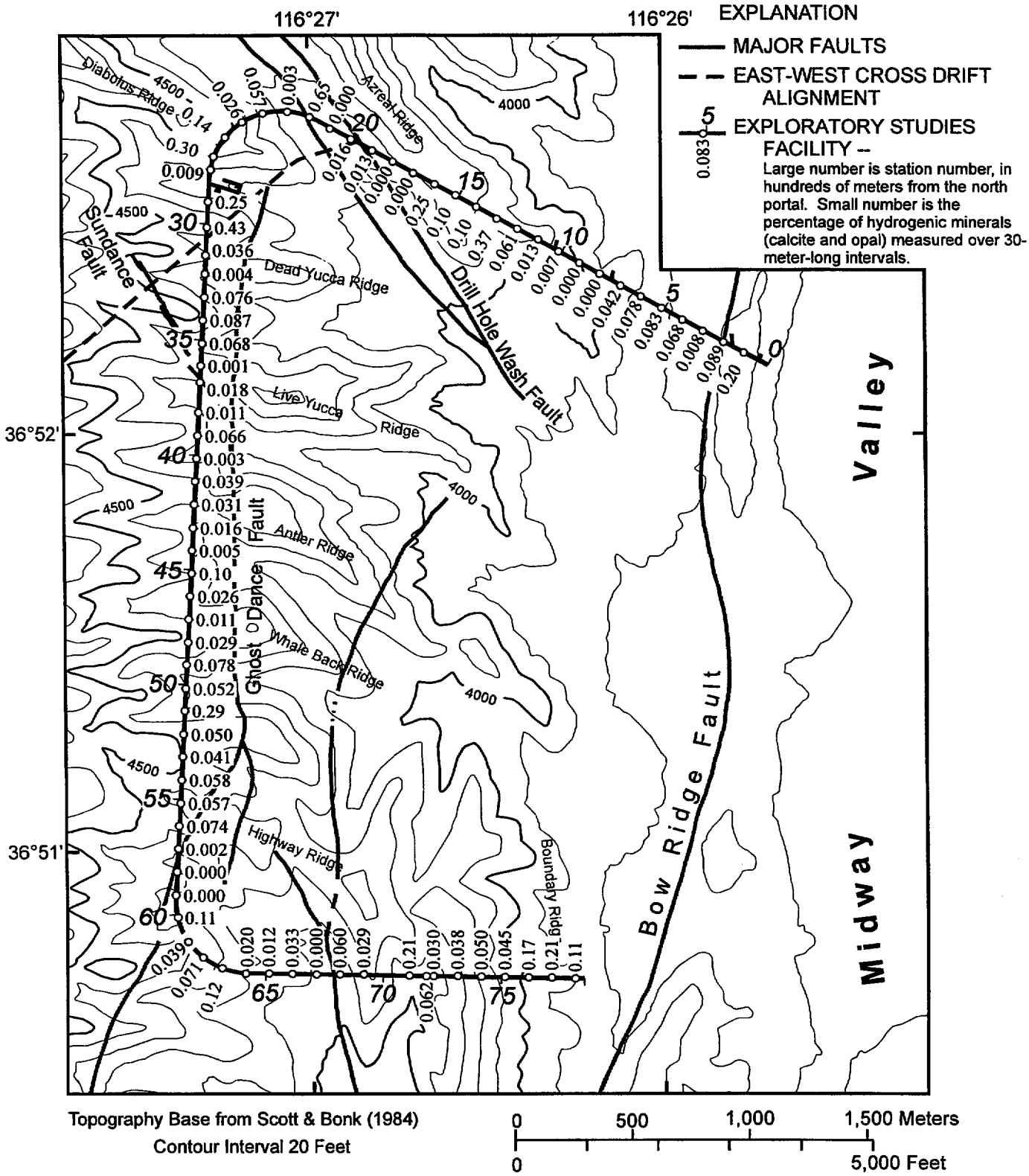

Figure 2. Map of the Exploratory Studies Facility and percentages of hydrogenic minerals, Yucca Mountain, Nevada.

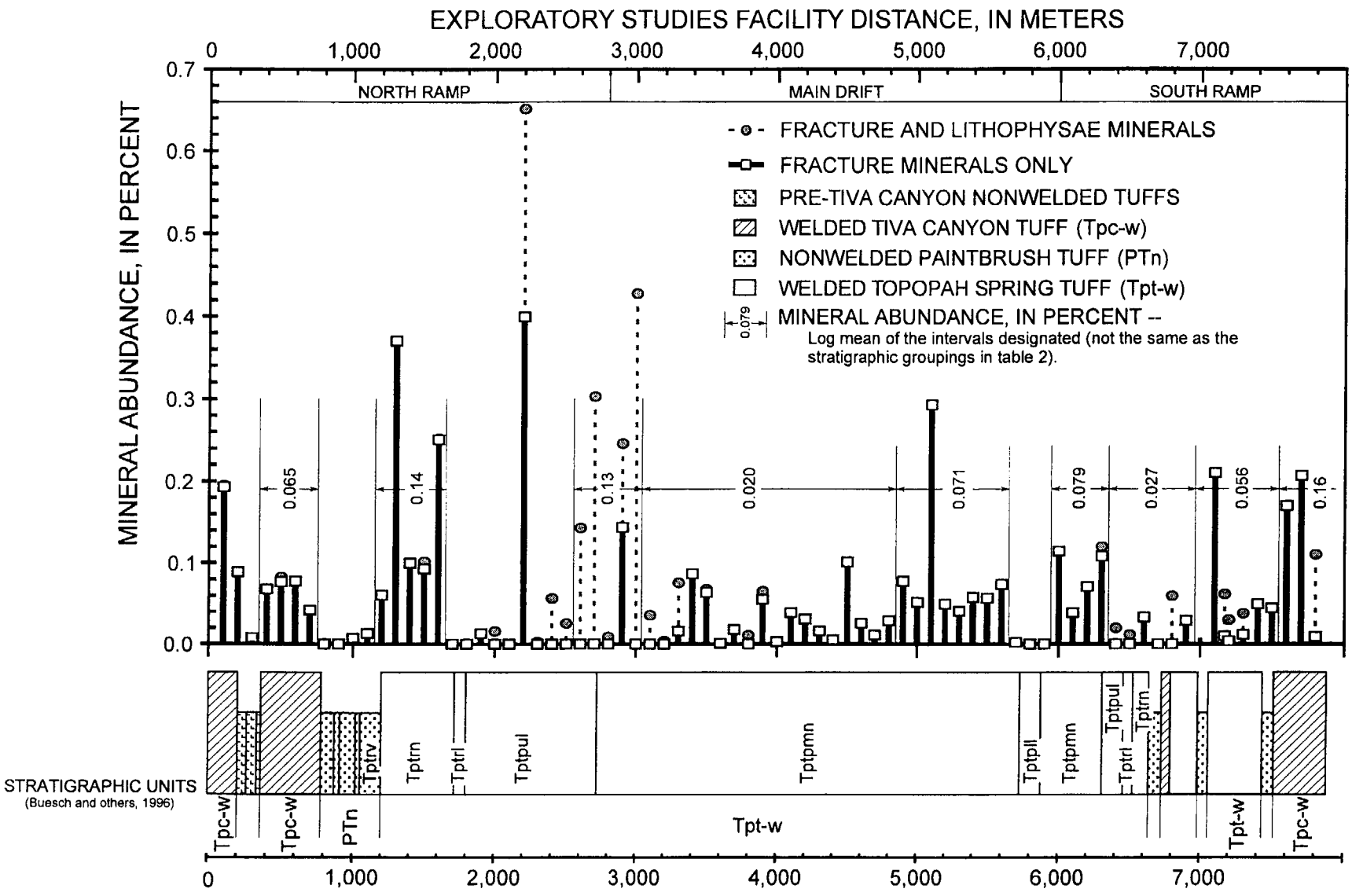

Figure 3. Hydrogenic-mineral abundances in the Exploratory Studies Facility plotted against distance from the north portal.

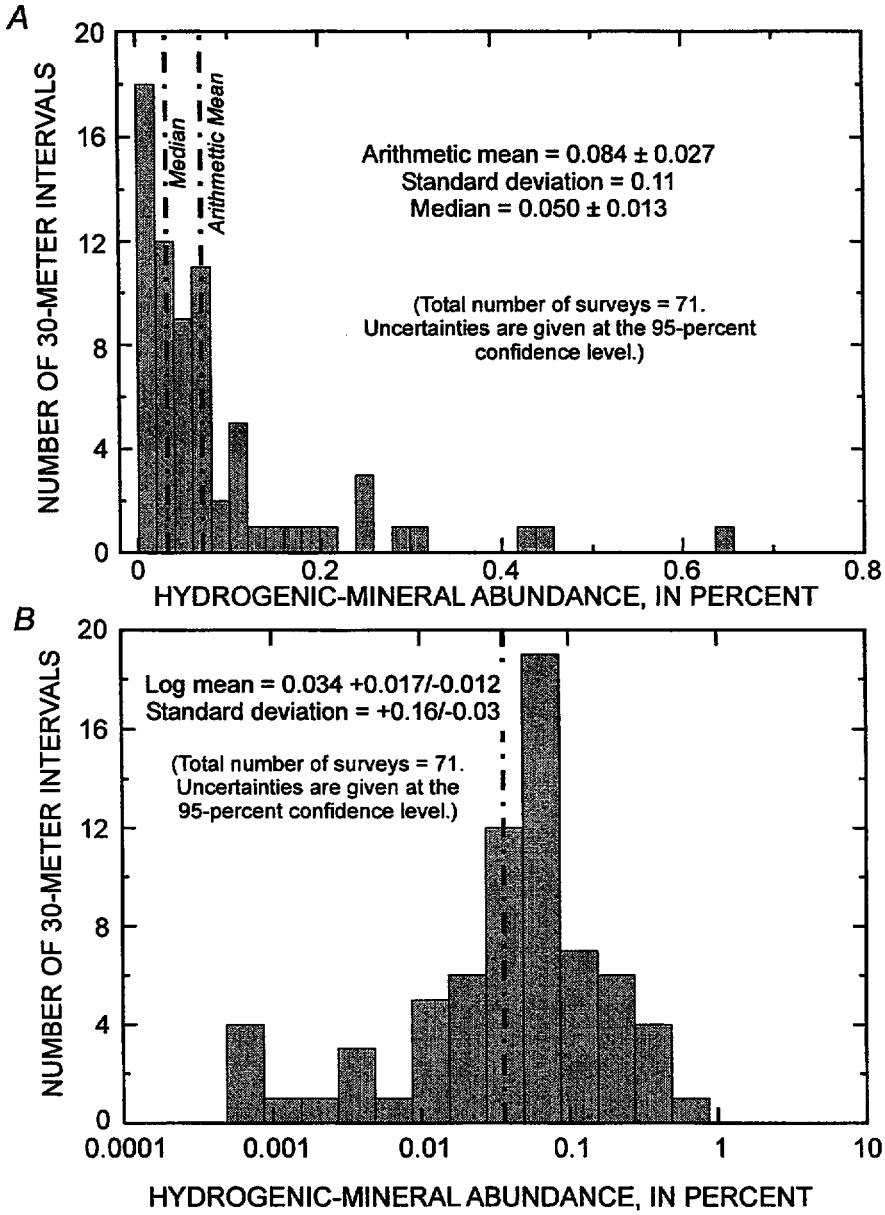

Figure 4. Histograms showing hydrogenic-mineral abundances in welded tuffs in the Exploratory Studies Facility on *A*, linear and *B*, log scales.

2ndMinAbund Hist - All.cdr

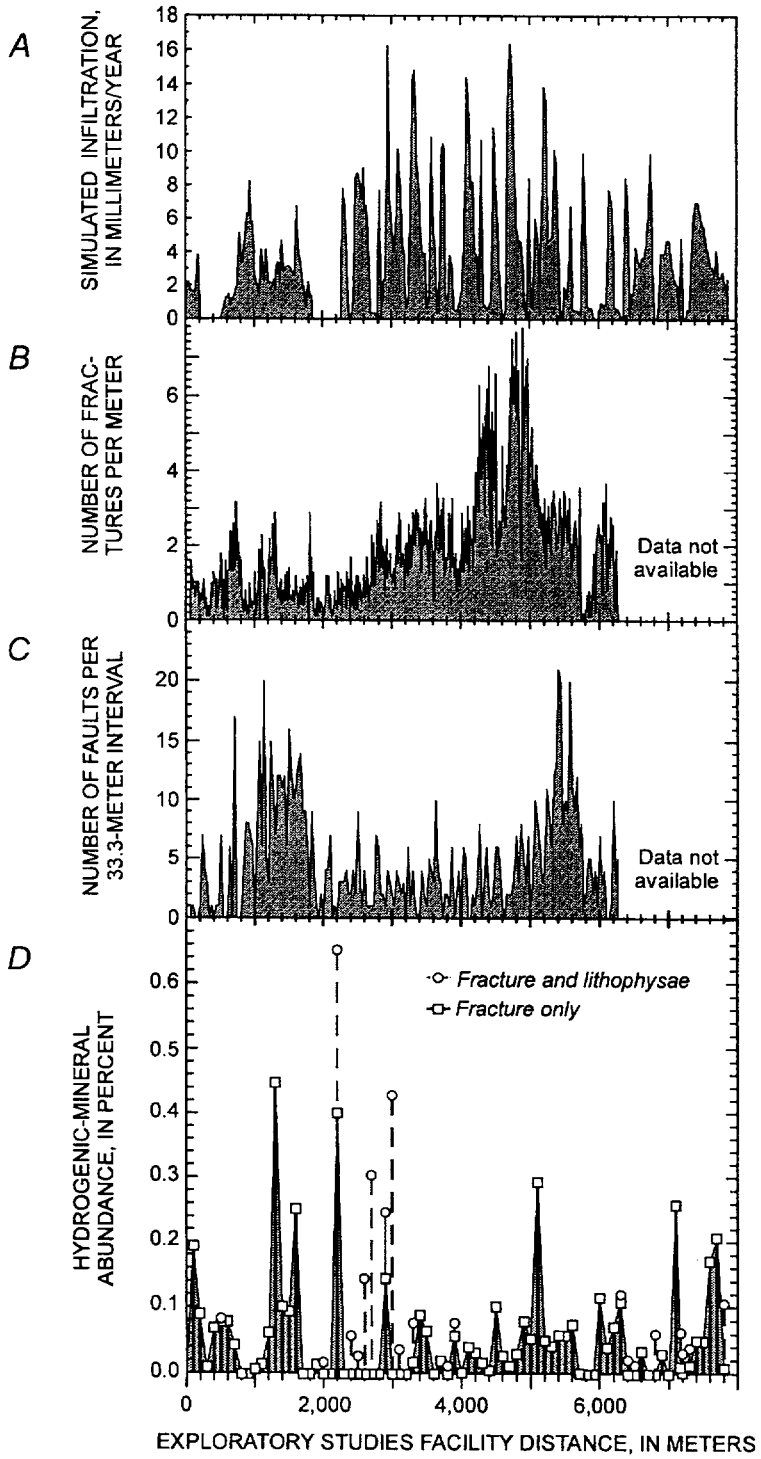

Figure 5. Estimates of *A,* simulated infiltration (A.L. Flint and others, U.S. Geological Survey, written commun., 1996); *B,* fracture density (S.C. Beason, Bureau of Reclamation, written commun., 1997); *C,* fault and shear density (S.C. Beason, Bureau of Reclamation, written commun., 1997); and *D,* hydrogenic-mineral abundance; plotted against distance from the north portal of the Exploratory Studies Facility.

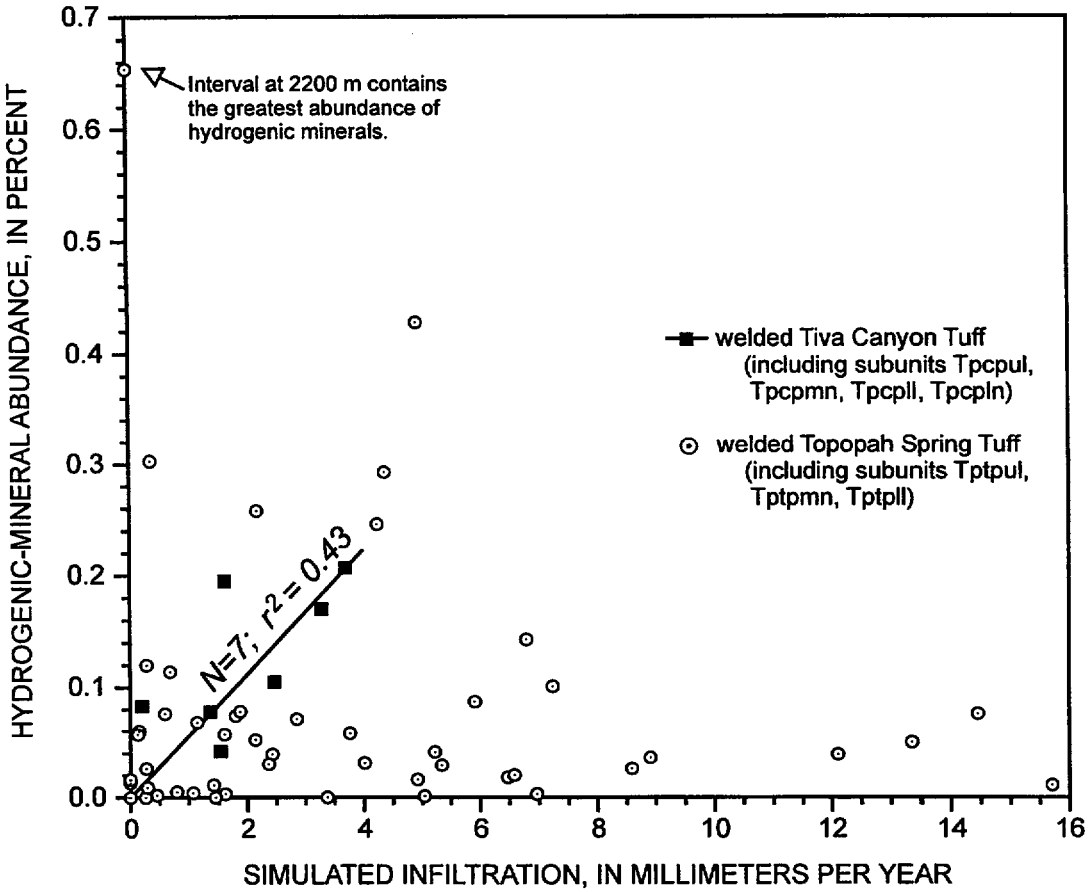

Figure 6. Hydrogenic-mineral abundance in the Exploratory Studies Facility and simulated infiltration (A.L. Flint and others, U.S. Geological Survey, written commun., 1996).

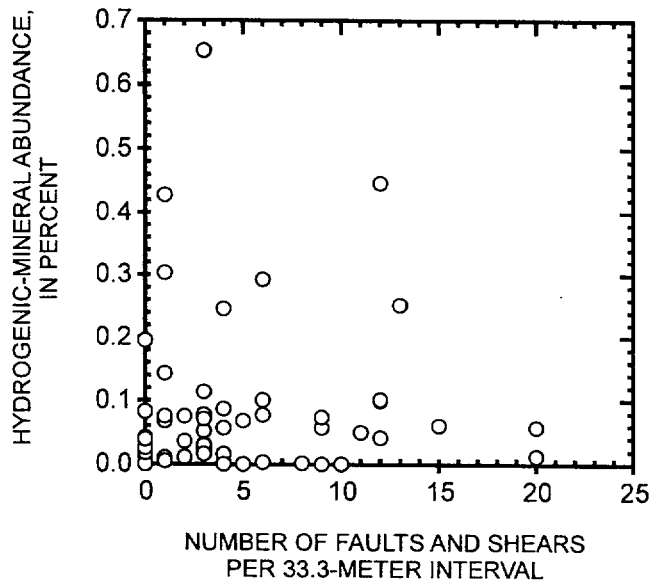

Figure 7. Hydrogenic-mineral abundance in welded units of the Topopah Spring Tuff and the number of faults and shears measured in the corresponding intervals in the Exploratory Studies Facility.

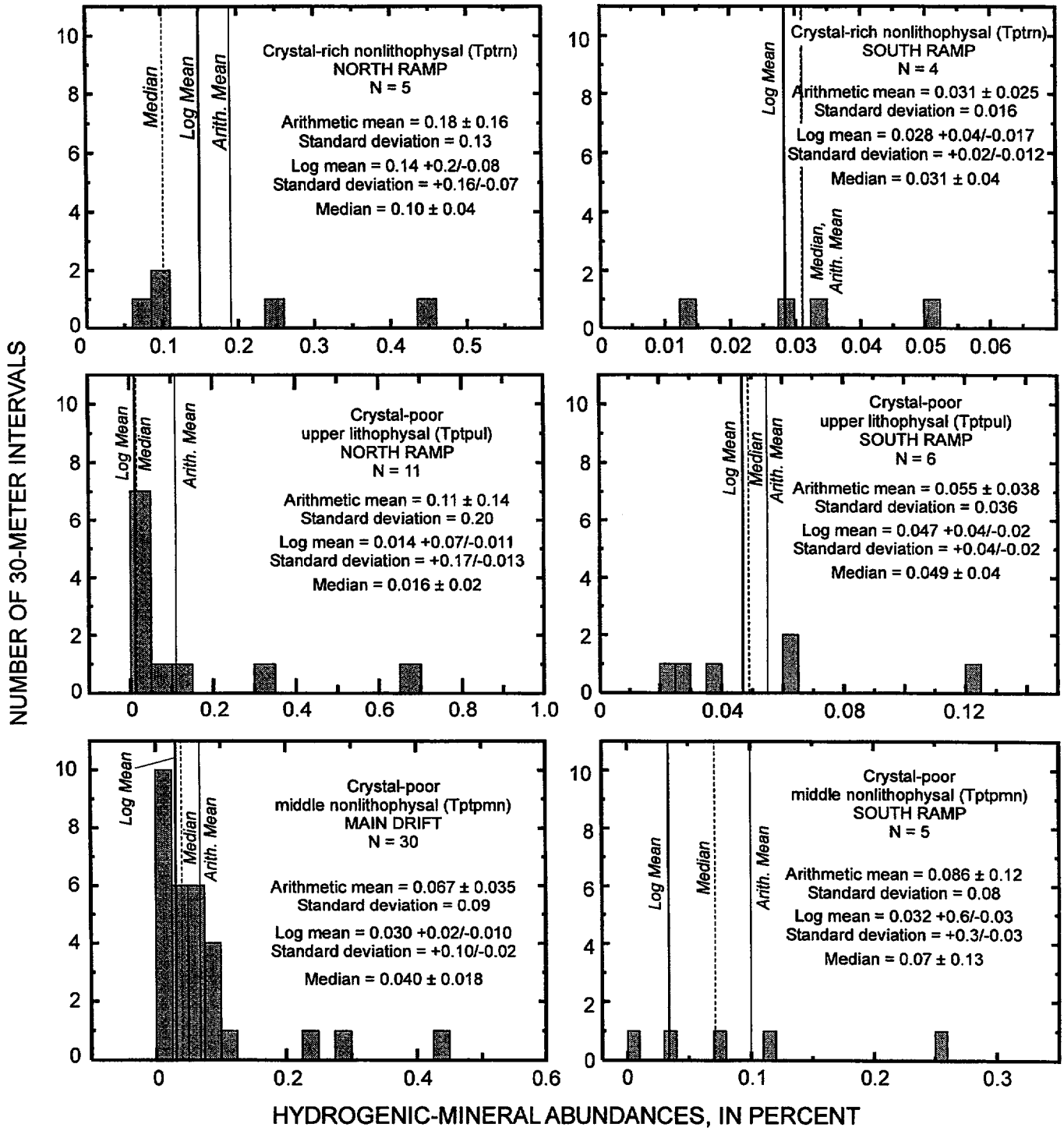

Figure 8. Histograms of hydrogenic-mineral abundances in three stratigraphic units of the Topopah Spring Tuff in the Exploratory Studies Facility. Uncertainties are reported as absolute errors quoted at the 95-percent confidence level.

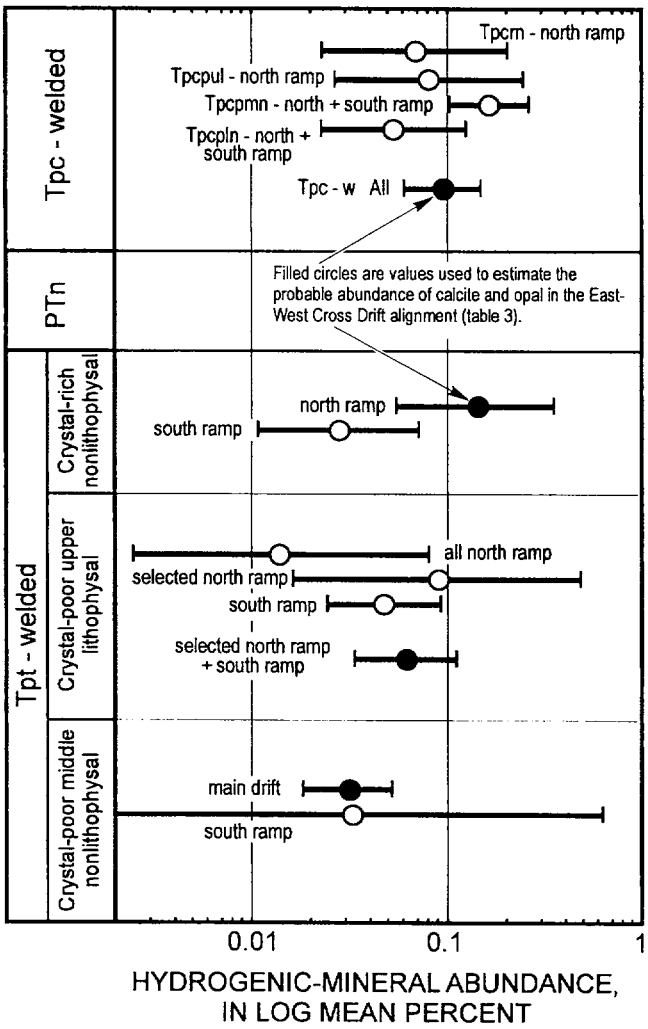

Figure 9. Summary of hydrogenic-mineral abundances in welded tuffs in the Exploratory Studies Facility. Stratigraphic units from Buesch and others (1996).

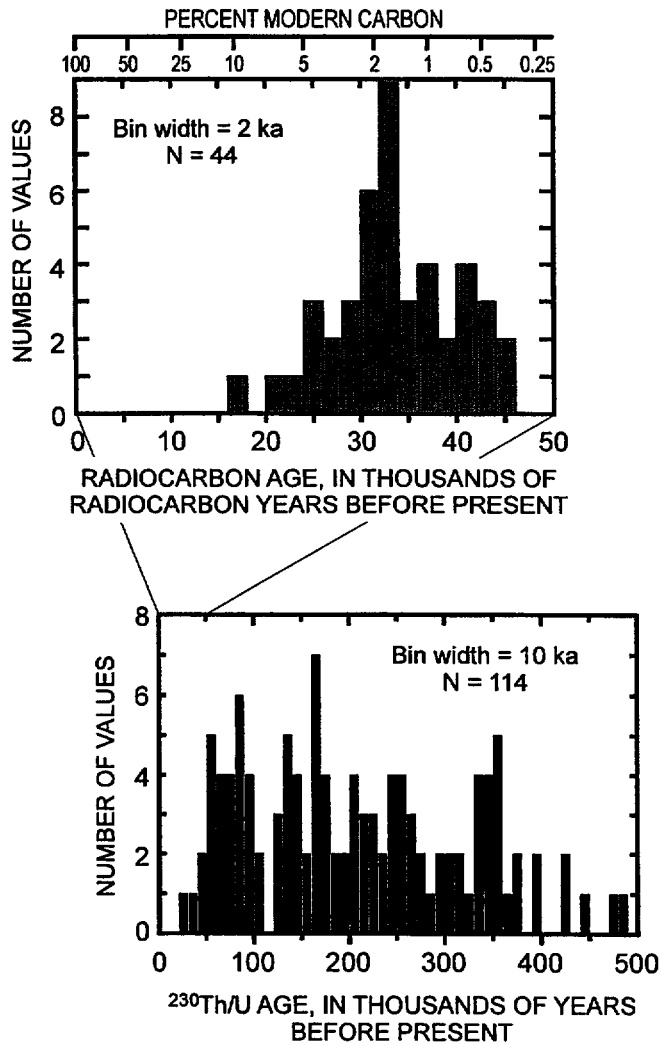

Figure 10. Histograms showing radiocarbon and thoruim-230/uranium (^{230}Th/U) ages for outer hydrogenic-mineral surfaces in the Exploratory Studies Facility.

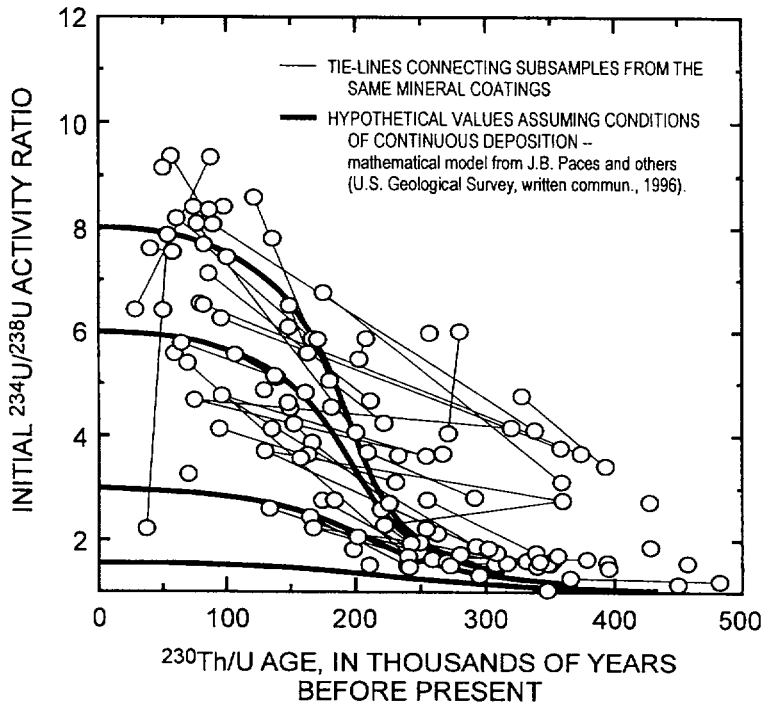

Figure 11. Covariance between initial uranium-234/uranium-238 ($^{234}U/^{238}U$) activity ratios and thorium-230/uranium ($^{230}Th/U$) ages for calcite and opal deposits in the Explorato Studies Facility.

AGE vs INITIAL - FIG 11.cdr

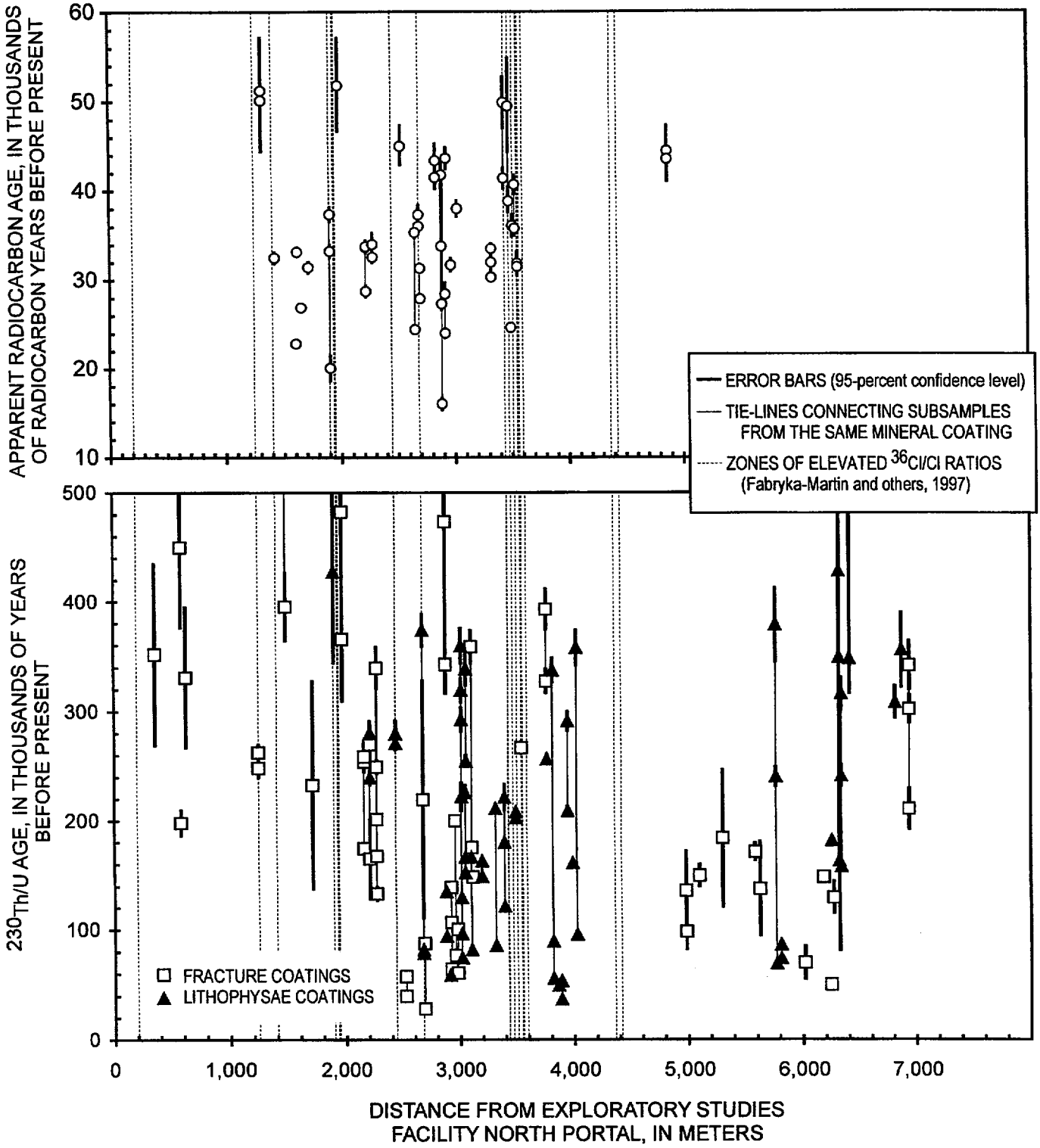

Figure 12. Distribution of radiocarbon and thorium-230/uranium (^{230}Th/U) ages for outer surfaces of hydrogenic minerals in the Exploratory Studies Facility.

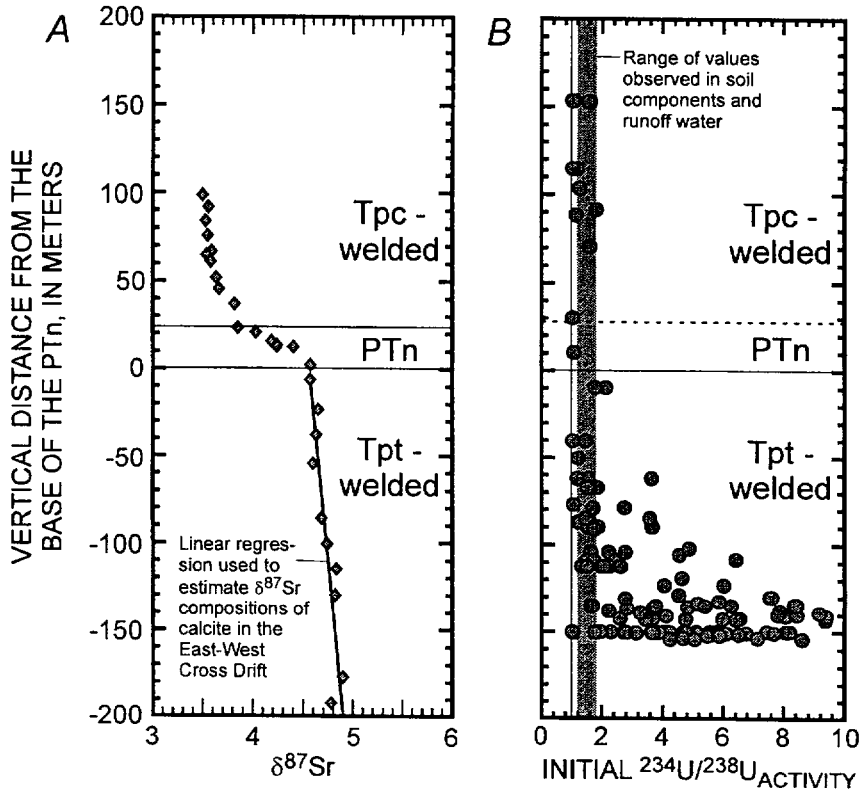

Figure 13. Variations of isotopic compositions plotted against vertical distance from the base of the Paintbrush Tuff nonwelded hydrogeologic unit for *A*, delta strontium-87 ($\delta^{87}Sr$) in pore water from borehole USW SD-7 (modified from Marshall and others, 1997) and *B*, initial uranium-234/uranium-238 ($^{234}U/^{238}U$) activity ratios for hydrogenic minerals from the Exploratory Studies Facility. Stratigraphic units from Buesch and others (1996).

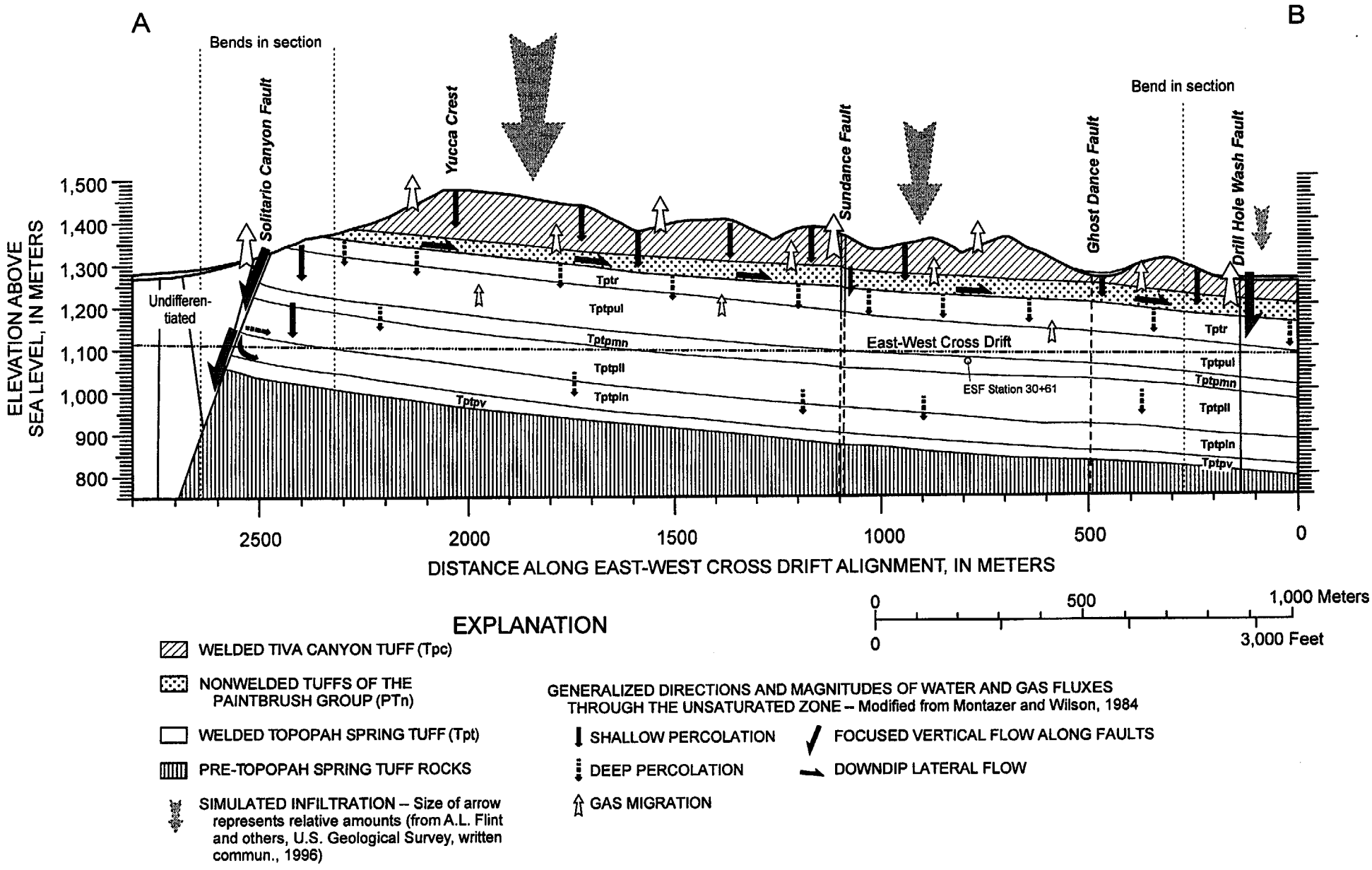

Figure 14. Geologic cross section of Yucca Mountain across the potential repository block along the alignment of the East-West Cross Drift (trace shown on fig. 1; modified from TRW Environmental Safety Systems, Inc., 1998). Stratigraphic units from Buesch and others (1996).

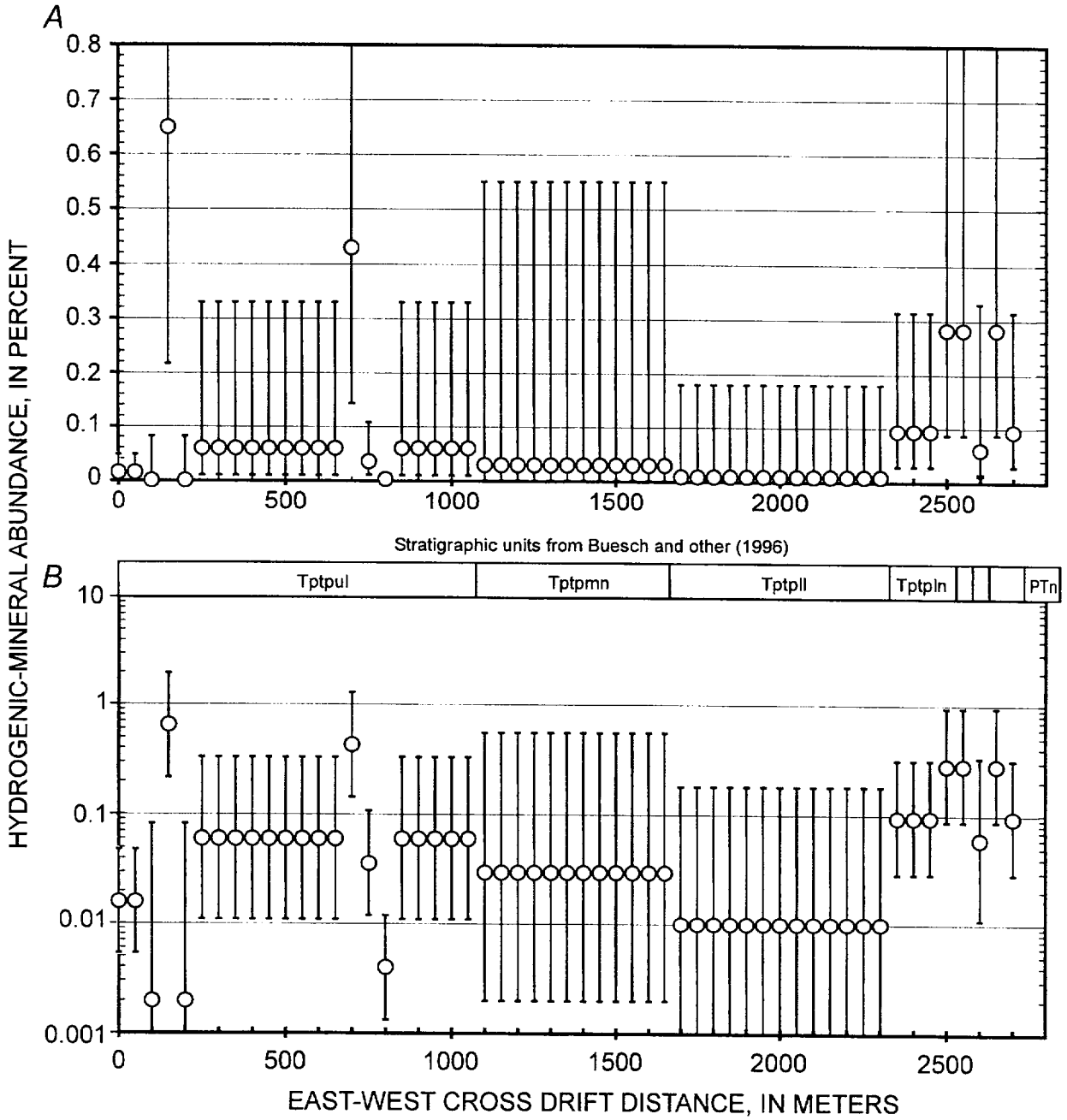

Figure 15. Hydrogenic-mineral abundances estimated for the East-West Cross Drift alignment plotted on *A*, linear and *B*, semilog scales with estimated uncertainties of two standard deviations.

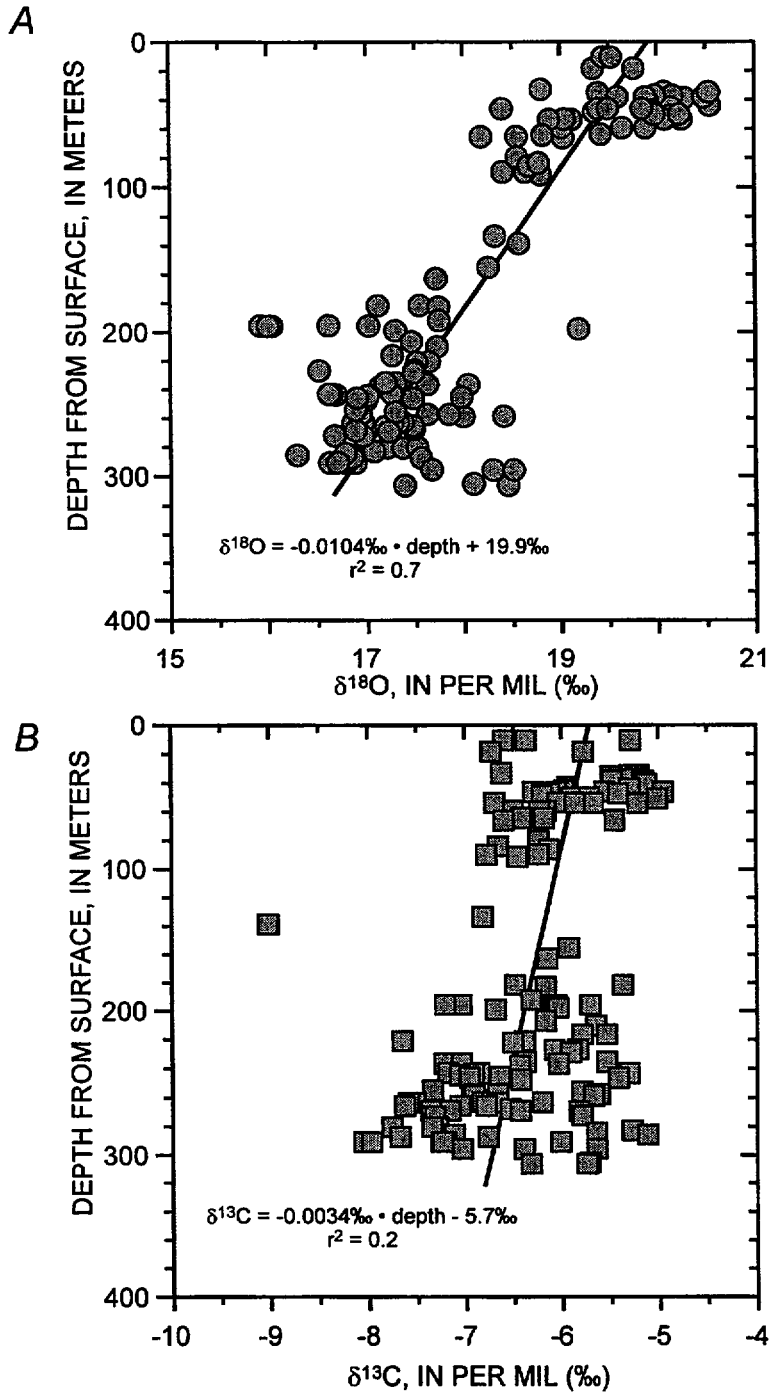

Figure 16. Depth from land surface plotted against *A*, delta oxygen-18 ($\delta^{18}O$) and *B*, delta carbon-13 ($\delta^{13}C$) for latest calcite deposits in the Exploratory Studies Facility.

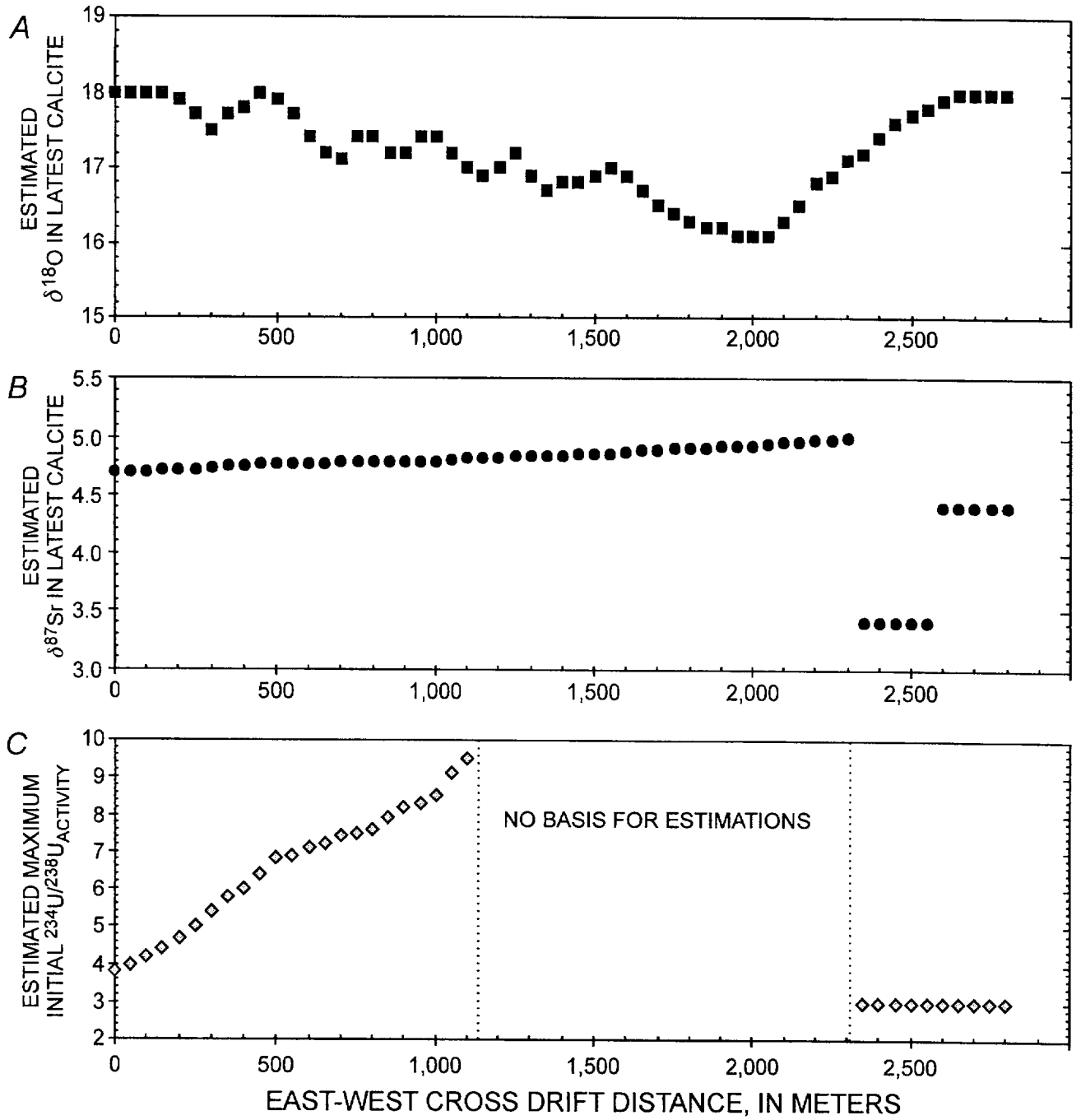

Figure 17. Estimates of *A*,delta oxygen-18 ($\delta^{18}O$), *B*, delta strontium-87 ($\delta^{87}Sr$), and *C*, maximum initial uranium-234/uranium-238 ($^{234}U/^{238}U$) activity ratios for hydrogenic minerals in the East-West Cross Drift alignment.

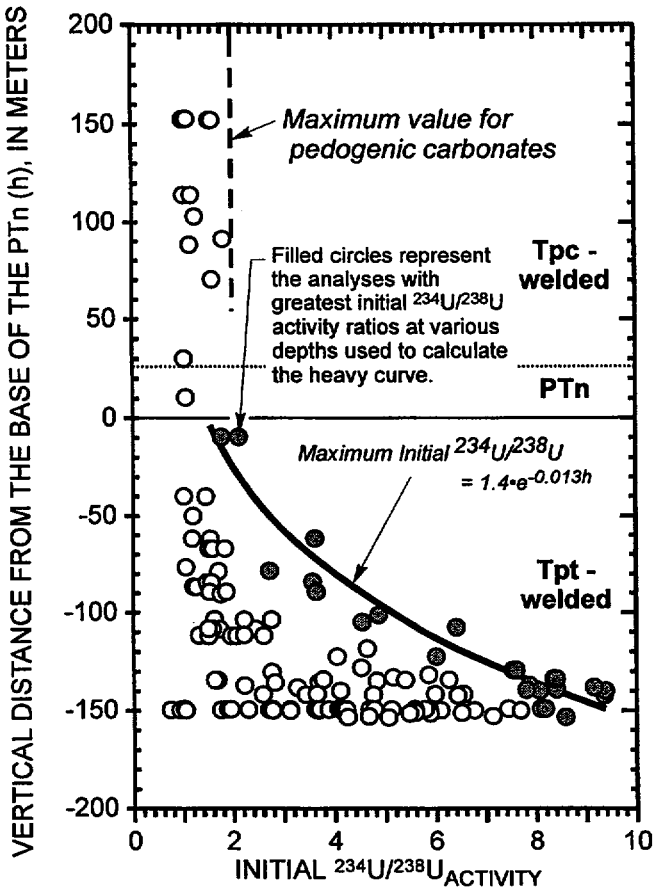

Figure 18. Initial uranium-234/uranium-238 ($^{234}U/^{238}U$) activity ratios for hydrogenic minerals from the Exploratory Studies Facility plotted against vertical distance from the base of the Paintbrush Tuff nonwelded hydrogeologic unit. Stratigraphic units from Buesch and others (1996).